

GSA Data Repository Items for Samperton *et al.*, “Zircon age–temperature–compositional spectra in plutonic rocks”.

1 Zircon geochronological–geochemical methods

Zircon trace element abundances (including [Ti] for Ti-in-zircon thermometry) were acquired using the UCLA CAMECA ims1270 and a $\sim 20 \mu\text{m}$ -diameter spot size, following the analytical procedure described by Storm *et al.* (2014) and calibrating all zircon trace element data against zircon standard 91500 (Liu *et al.*, 2010). Trends in Bergell zircon compositional proxies (Th/U, Ce/Ce*, Lu/Hf; e.g., Ballard *et al.*, 2002) as a function of temperature are observed for tonalite samples BR10-04 and -03, while trends are not observed for granodiorite sample BR11-03 (Figs. 2, DR1). CL image compilations for zircons analyzed by SIMS are shown in Figs. DR2–4. No correlation in degree of zircon alteration as a function of Ti-in-zircon temperature is observed (Fig. DR5; Bell *et al.*, 2016), supporting interpretation of Ti-in-zircon data as robust crystallization temperatures. Raw SIMS data are given in Table DR1 and reduced Ti-in-zircon thermometric data are given in Table DR2.

U–Pb zircon CA-ID-TIMS-TEA analyses were performed following the analytical protocol described in detail by Samperton *et al.* (2015), with complete data tables contained therein. CL images for zircons analyzed by U–Pb zircon CA-ID-TIMS-TEA are shown in Figs. DR6–11. Data corresponding to primary magmatic zircon domains interpreted by Samperton *et al.* (2015) and used in the current study are given in Table DR3. In calculating the cumulative zircon age distributions in Fig. 4, we employ an approach wherein the weight assigned to a given U–Pb date is proportional to the zircon’s size. A mixture of microsampling sub-crystal domains versus conventional single-grain analyses in this study results in a wide range of sampling sizes (e.g., Fig. DR6). In order to more accurately relate a given U–Pb date to the amount of zircon crystallized at that time, the cross-sectional area of each grain (A_i) was measured from CL images (unit: μm^2 ; given in last column of Table DR3). The total cross-sectional area of zircon in a given sample (A_T) was determined by summing all values of A_i . The weight ω_i applied to a given U–Pb date is set by the quotient of A_i and A_T , such that for n total primary magmatic U–Pb dates in a given sample,

$$\sum_{i=1}^n \frac{A_i}{A_T} = \sum_{i=1}^n \frac{A_i}{A_1 + A_2 + \dots + A_{n-1} + A_n} = \sum_{i=1}^n \omega_i = 1 \quad (1)$$

The intent of this operation is to place greater weight on larger zircon domains (e.g., whole single crystals) relative to smaller zircon domains (e.g., microsampled crystal tips), as U–Pb dates from the former integrate a larger mass of zircon than the latter. In this study, heterogeneous sample size is unique to CA-ID-TIMS as there is greater flexibility in this regard compared to *in situ* methods like SIMS, where sampling volume is standardized throughout. This point is succinctly illustrated by comparing the radiogenic Pb content (Pb^*) of each U–Pb zircon CA-ID-TIMS analysis (i.e., a proxy for grain size) to the grain size measurements described above (Fig. DR14), where a good first-order

positive correlation is observed as anticipated. Differences in the distributions of weighted versus unweighted U–Pb zircon age spectra are also apparent in kernel density estimate plots (Fig. DR15), further underscoring the importance of accounting for heterogeneous sampling sizes when quantifying high-precision geochronological datasets.

Magmatic cooling rates were calculated using the observed spread in U–Pb zircon CA-ID-TIMS dates for samples BR10-04 and -03 (609 ± 90 and 706 ± 57 kyr, respectively) and the difference in Ti-in-zircon temperature between the lowest-T/lowest-Th/U and highest-T/highest-Th/U analyses in a given sample (164 ± 29 and 89 ± 34 °C, respectively). Dividing the latter by the former yields respective supersolidus cooling rates of 269 ± 62 and 126 ± 50 °C/Myr (2σ).

2 MELTS zircon crystallization distributions and $aTiO_2$ modeling

Model zircon crystallization distributions were calculated from MELTS major-element batch crystallization simulations using the saturation model of Boehnke *et al.* (2013) and the numerical approach developed by Keller *et al.* (2015). Whole-rock compositions of samples BR10-04 and -03 (determined by Actlabs and given in Table DR4) were used as starting liquid compositions at 6.6 and 6.9 kbar, respectively, corresponding to magma emplacement depths from Al-in-hornblende barometry (Reusser, 1987; Davidson *et al.*, 1996). The calculated melt Zr concentration ($[Zr]_{calc}^{melt}$) of each simulation step was determined using MELTS modal mineral abundances and Zr partition coefficients compiled from the Geochemical Earth Reference Model (GERM; <https://earthref.org/GERM/>). Concurrently, the zircon solubility model of Boehnke *et al.* (2013) was used to calculate the melt Zr concentration required for zircon saturation ($[Zr]_{sat}^{melt}$) under the system T–P–X conditions of each simulation step. In this model, the compositional proxy $M = (Na+K+2Ca)/(Al+Si)$ (molar, normalized element components) was used as a compositional proxy for system growth/dissolution of zircon. Zircon growth initiated when $[Zr]_{calc}^{melt} > [Zr]_{sat}^{melt}$ and continued to the solidus, and the mass of zircon crystallized was determined at each simulation interval to produce a distribution of zircon growth as a function of temperature and melt fraction (Fig. DR16). A total of 5000 Monte Carlo simulations were performed in which magmatic H₂O content was varied between 0–10 wt.%, and major element oxide compositions were resampled within a conservative ± 3 wt.% (2σ) range of their nominal whole-rock compositions. The former operation was performed to account for uncertainty in initial magmatic H₂O content during crystallization, and the latter to ensure that simulations do not underrepresent the variability in potential crystallization/differentiation paths. Results were binned in 2.5 wt.% H₂O increments to produce the average distributions shown in Figure 3. Results of 7.5–10 wt.% H₂O simulations were omitted from Figs. 3 and 4 for clarity.

TiO₂ activity ($aTiO_2$) was calculated using the rutile solubility model of Hayden and Watson (2007) and the MELTS major-element batch crystallization simulations described above under water-saturated conditions (Fig. DR17), with mean values used to calculate absolute Ti-in-zircon temperatures presented in Figure 3. Full source code can be found at the following URL: <https://github.com/brehinkeller/StatisticalGeochemistry>

In addition, we present the results of MELTS crystallization simulations on a database of volcanic whole-rock

geochemistry below (from Keller et al., 2015, *Nature*, doi: [10.1038/nature14584](https://doi.org/10.1038/nature14584); Fig. DR18). This plot shows the average zircon saturation temperature for whole-rock compositions binned at 2.5-wt% SiO₂ intervals. It is clear from the figure that for a given SiO₂ content, the Watson and Harrison model yields zircon saturation temperatures ~50–70 °C greater than that of Boehnke et al. (and even more so for very mafic compositions). As noted in the manuscript, MELTS has been observed empirically to overestimate actual temperatures by ~25–50 °C; when this bias is accounted for, excellent consistency is observed between Ti-in-zircon data and MELTS zircon crystallization simulations using the solubility model of Boehnke et al. However, use of the Watson and Harrison model yields MELTS zircon crystallization temperatures ~50–70 °C too hot still, even after making a bias correction. Such a discrepancy in our opinion indicates an issue with the calibration of Watson and Harrison, and we therefore prefer the model of Boehnke et al.

References

- Ballard, J.R., Palin, J.M., and Campbell, I.H., 2002, Relative oxidation states of magmas inferred from Ce(IV)/Ce(III) in zircon: application to porphyry copper deposits of northern Chile: *Contributions to Mineralogy and Petrology*, vol. 144, pp. 347–364, doi:10.1007/s00410-002-0402-5.
- Bell, E.A., Boehnke, P., and Harrison, T.M., 2016, Recovering the primary geochemistry of Jack Hills zircons through quantitative estimates of chemical alteration: *Geochimica et Cosmochimica Acta*, vol. 191, pp. 187–202, doi:10.1016/j.gca.2016.07.016.
- Boehnke, P., Watson, E.B., Trail, D., Harrison, T.M., and Schmitt, A.K., 2013, Zircon saturation re-revisted: *Chemical Geology*, vol. 351, pp. 324–334, doi:10.1016/j.chemgeo.2013.05.028.
- Davidson, C., Rosenberg, C., and Schmid, S.M., 1996, Synmagmatic folding of the base of the Bergell pluton, Central Alps: *Tectonophysics*, vol. 265, pp. 213–238, doi:10.1016/S0040-1951(96)00070-4.
- Hayden, L.A. and Watson, E.B., 2007, Rutile saturation in hydrous siliceous melts and its bearing on Ti-thermometry of quartz and zircon: *Earth and Planetary Science Letters*, vol. 258, pp. 561–568, doi:10.1016/j.epsl.2007.04.020.
- Hürlimann, N., Müntener, O., Ulmer, P., Nandedkar, R., Chiaradia, M., and Ovtcharova, M., 2016, Primary magmas in continental arcs and their differentiated products: Petrology of a post-plutonic dyke suite in the Tertiary Adamello batholith (Alps): *Journal of Petrology*, vol. 57, pp. 495–534, doi:10.1093/petrology/egw016.
- Keller, C.B., Schoene, B., and Boehnke, P., 2015, Temporal variation in average zircon saturation temperature over last 4 Gyr: *Goldschmidt Abstracts*, p. 1545.
- Liu, Y., Hu, Z., Zong, K., Gao, C., Gao, S., Xu, J., and Chen, H., 2010, Reappraisal and refinement of zircon U–Pb isotope and trace element analyses by LA-ICP-MS: *Chinese Science Bulletin*, vol. 55, pp. 1535–1546, doi:10.1007/s11434-010-3052-4.
- Reusser, E., 1987, Phasenbeziehungen im Tonalit der Bergeller Intrusion: Ph.D. thesis, ETH-Zürich, doi:10.3929/ethz-a-000475536, 220 pp.
- Samperton, K.M., Schoene, B., Cottle, J.M., Keller, C.B., Crowley, J.L., and Schmitz, M.D., 2015, Magma emplacement, differentiation and cooling in the middle crust: Integrated zircon geochronological–geochemical constraints from the Bergell Intrusion, Central Alps: *Chemical Geology*, vol. 417, pp. 322–340, doi:10.1016/j.chemgeo.2015.10.024.

Storm, S., Schmitt, A.K., Shane, P., and Lindsay, J.M., 2014, Zircon trace element chemistry at sub-micrometer resolution for Tarawera volcano, New Zealand, and implications for rhyolite magma evolution: *Contributions to Mineralogy and Petrology*, vol. 167, doi:10.1007/s00410-014-1000-z.

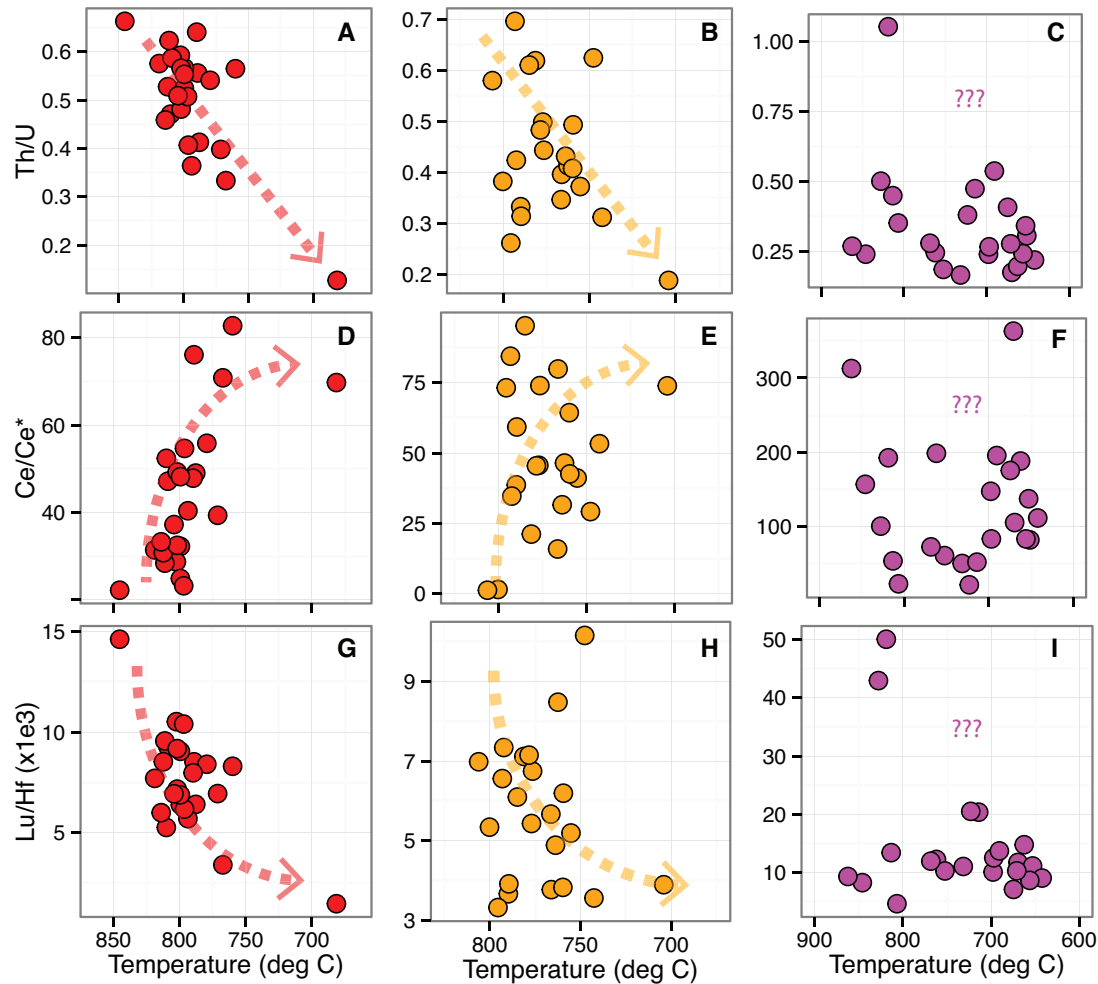


Figure DR1. T-X crossplots of zircon Th/U, cerium anomaly (Ce/Ce*) and Lu/Hf as a function of Ti-in-zircon crystallization temperature for tonalite samples BR10-04 (A,D,G) and -03 (B,E,H), and granodiorite sample BR11-03 (C,F,I). Tonalites show broadly decreasing Th/U and Lu/Hf, and increasing Ce/Ce*, with decreasing temperature (i.e., increasing differentiation), while granodioritic zircons show no such systematic trends. Data obtained by SIMS microanalysis.

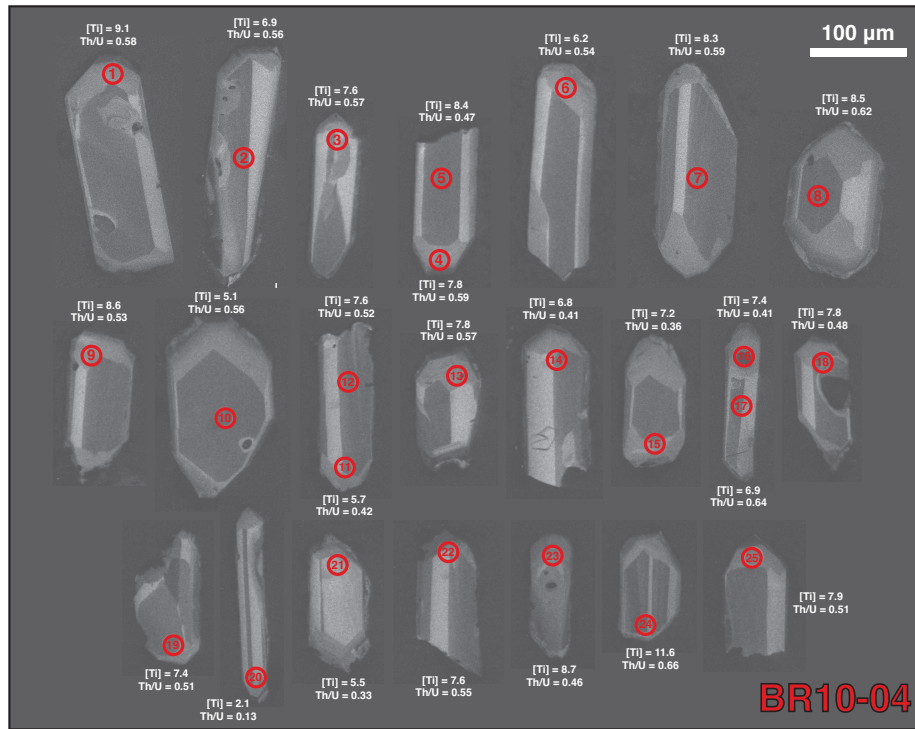


Figure DR2. CL images of BR10-04 zircons characterized by SIMS, with [Ti] and Th/U of each spot (n=25) indicated.

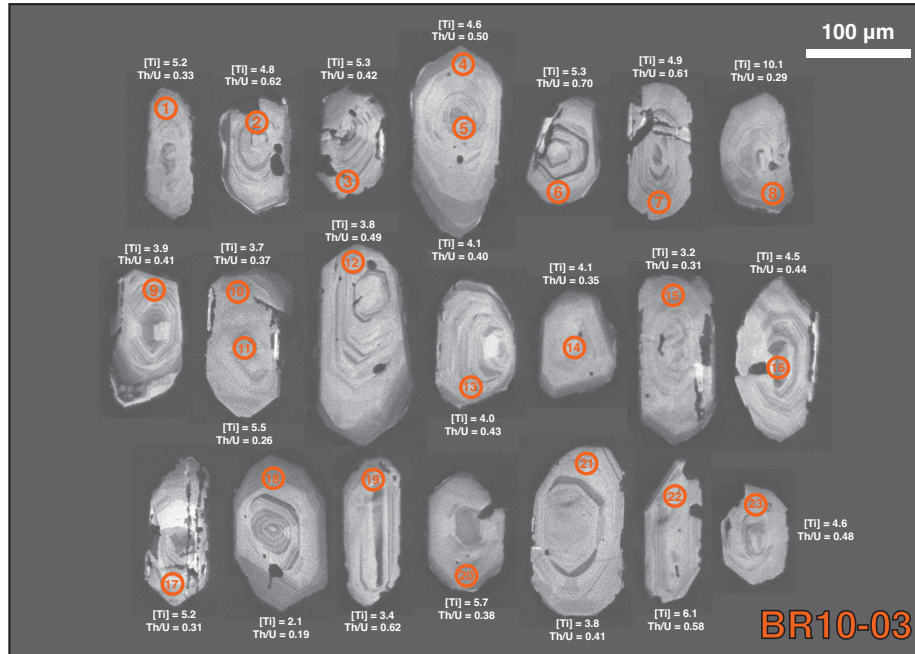


Figure DR3. CL images of BR10-03 zircons characterized by SIMS, with [Ti] and Th/U of each spot (n=23) indicated.



Figure DR4. CL images of BR11-03 zircons characterized by SIMS, with [Ti] and Th/U of each spot (n=23) indicated.

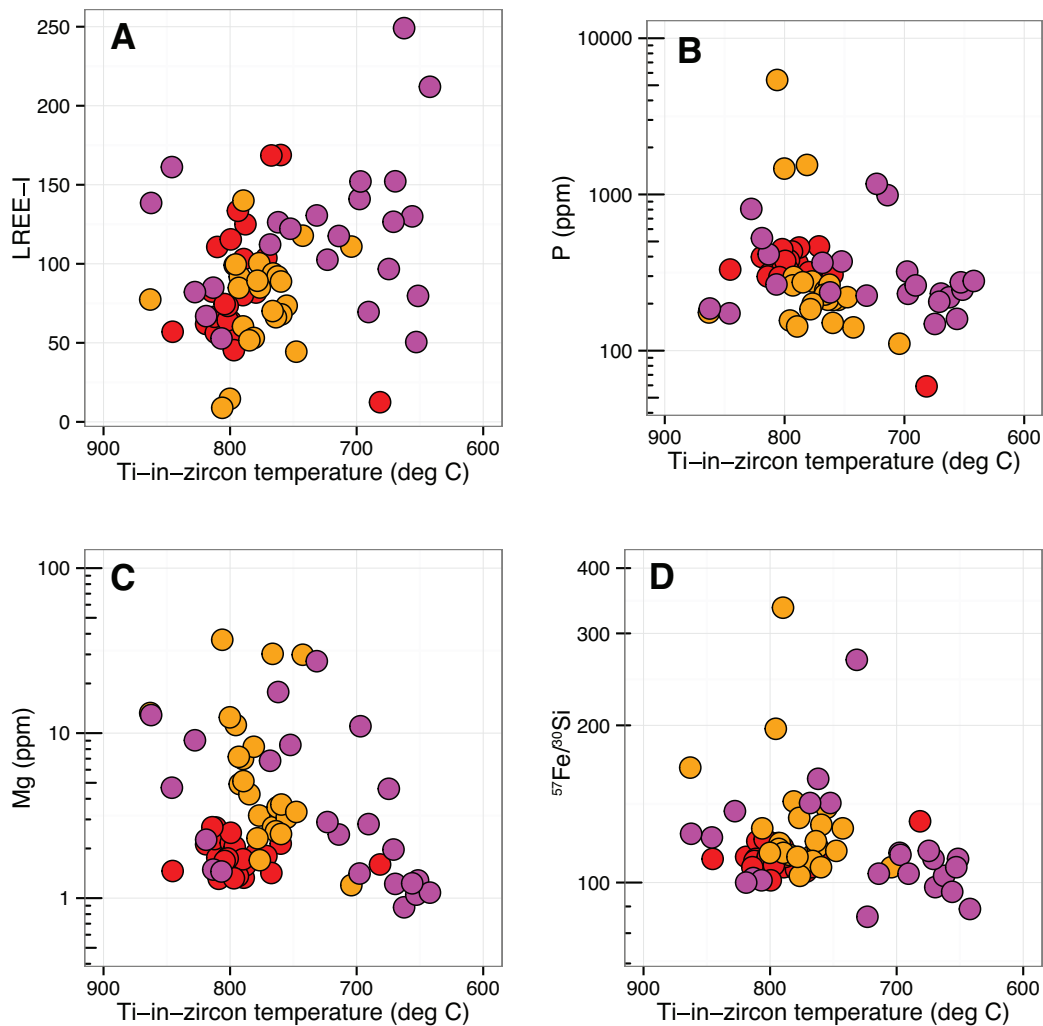


Figure DR5. Plots of various alteration indices as a function of Ti-in-zircon temperature from SIMS microanalyses, including LREE-I (A; Bell *et al.*, 2016), phosphorus (B), magnesium (C), and iron-to-silicon ratio (D). The absence of trends in apparent degree of alteration with temperature supports the fidelity of Ti-in-zircon thermometric data as recording primary magmatic temperature evolution.

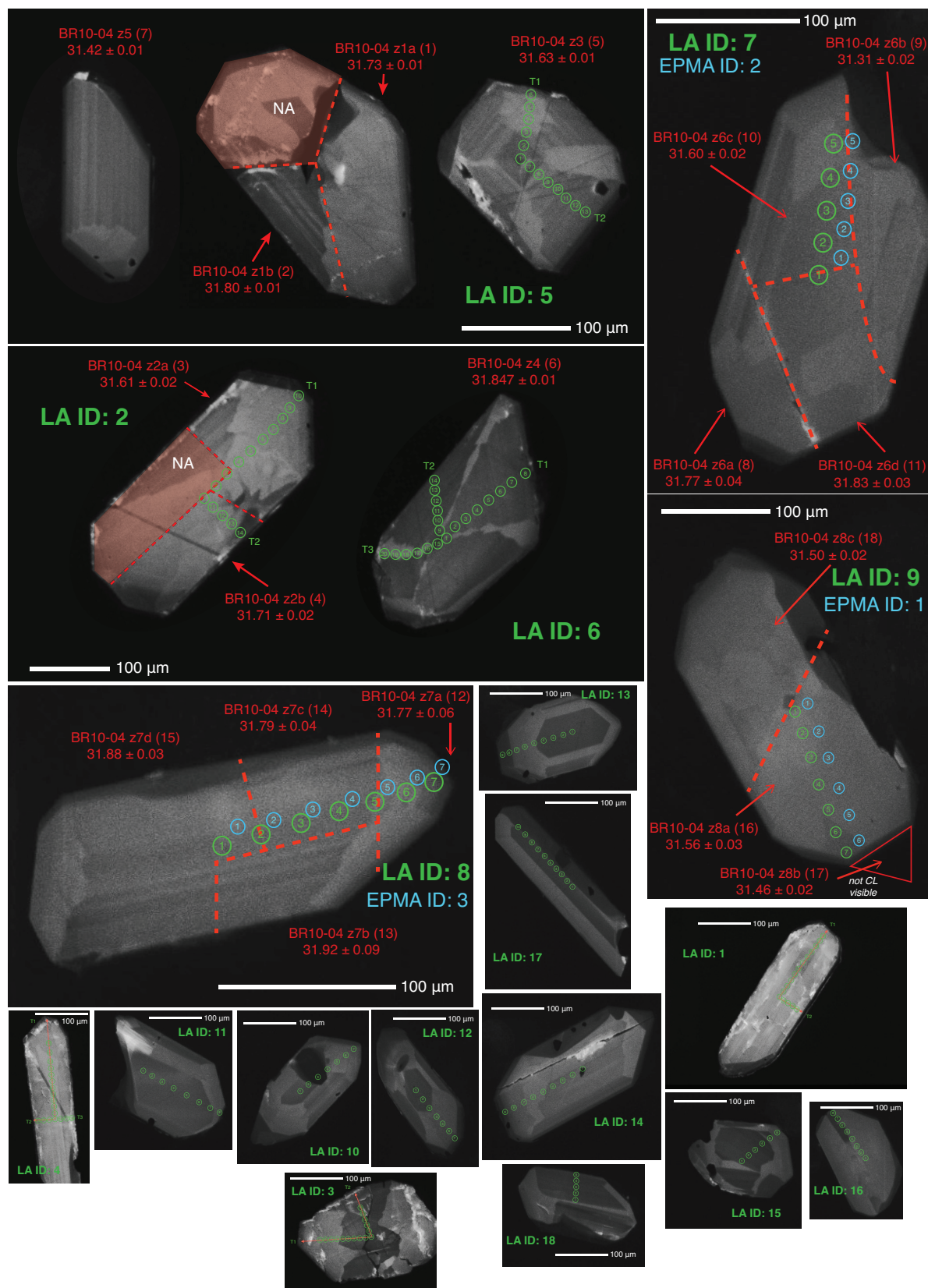


Figure DR6. BR10-04 CL images with LA-ICPMS transect points (green numbers+circles), EPMA points (blue numbers+circles), and U-Pb TIMS-TEA fragment boundaries (dashed red lines). U-Pb TIMS-TEA grain/fragment IDs+dates correspond to data in Table DR3. 18 U-Pb TIMS-TEA analyses, 192 LA-ICPMS points/26 transects/18 grains. Images and data reproduced from Samperton et al. (2015).

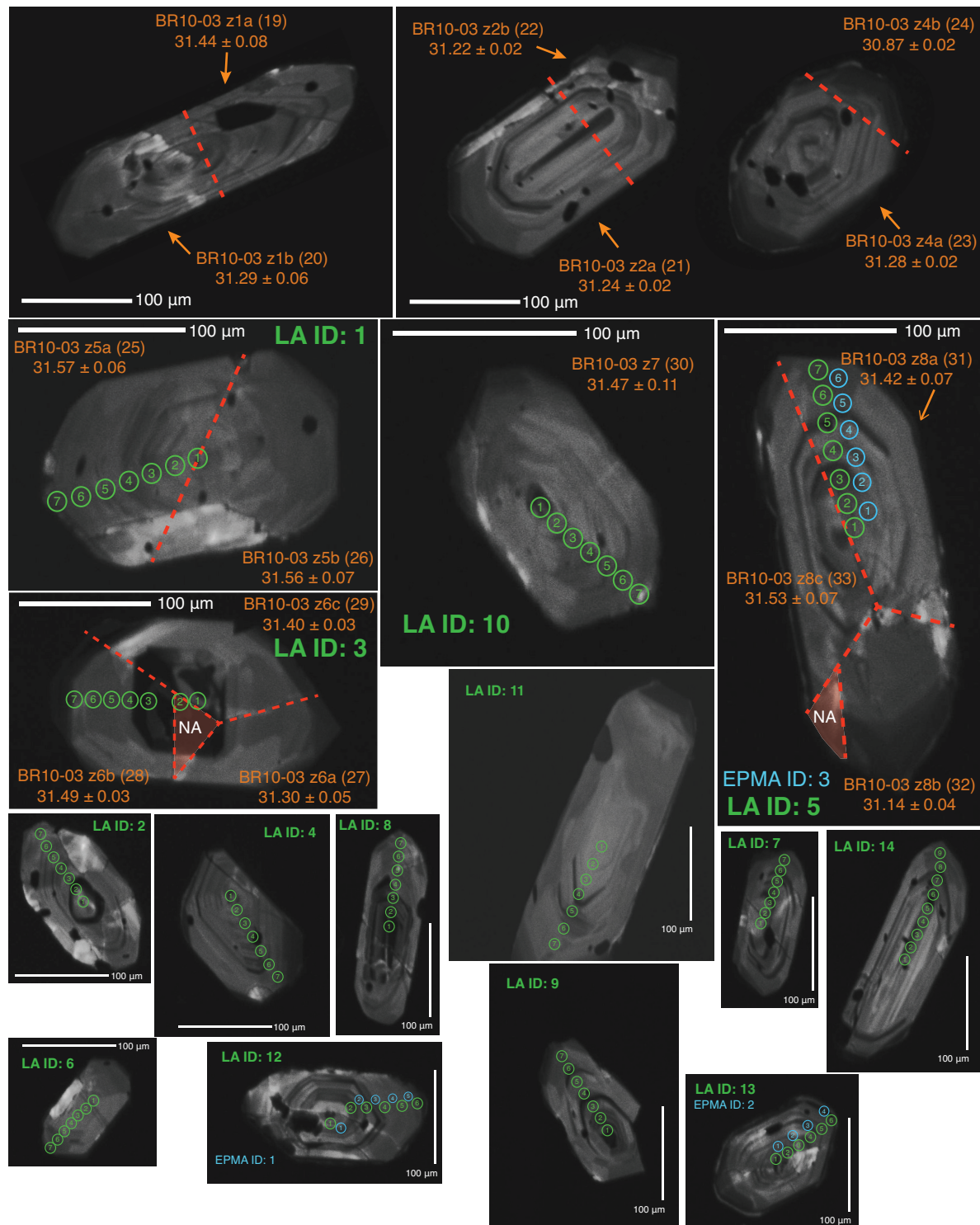


Figure DR7. BR10-03 CL images with LA-ICPMS transect points (green numbers+circles), EPMA points (blue numbers+circles), and U-Pb TIMS-TEA fragment boundaries (dashed red lines). U-Pb TIMS-TEA grain/fragment IDs+dates correspond to data in Table DR3. 15 U-Pb TIMS-TEA analyses, 98 LA-ICPMS points/14 transects/14 grains. Images and data reproduced from Samperton et al. (2015).

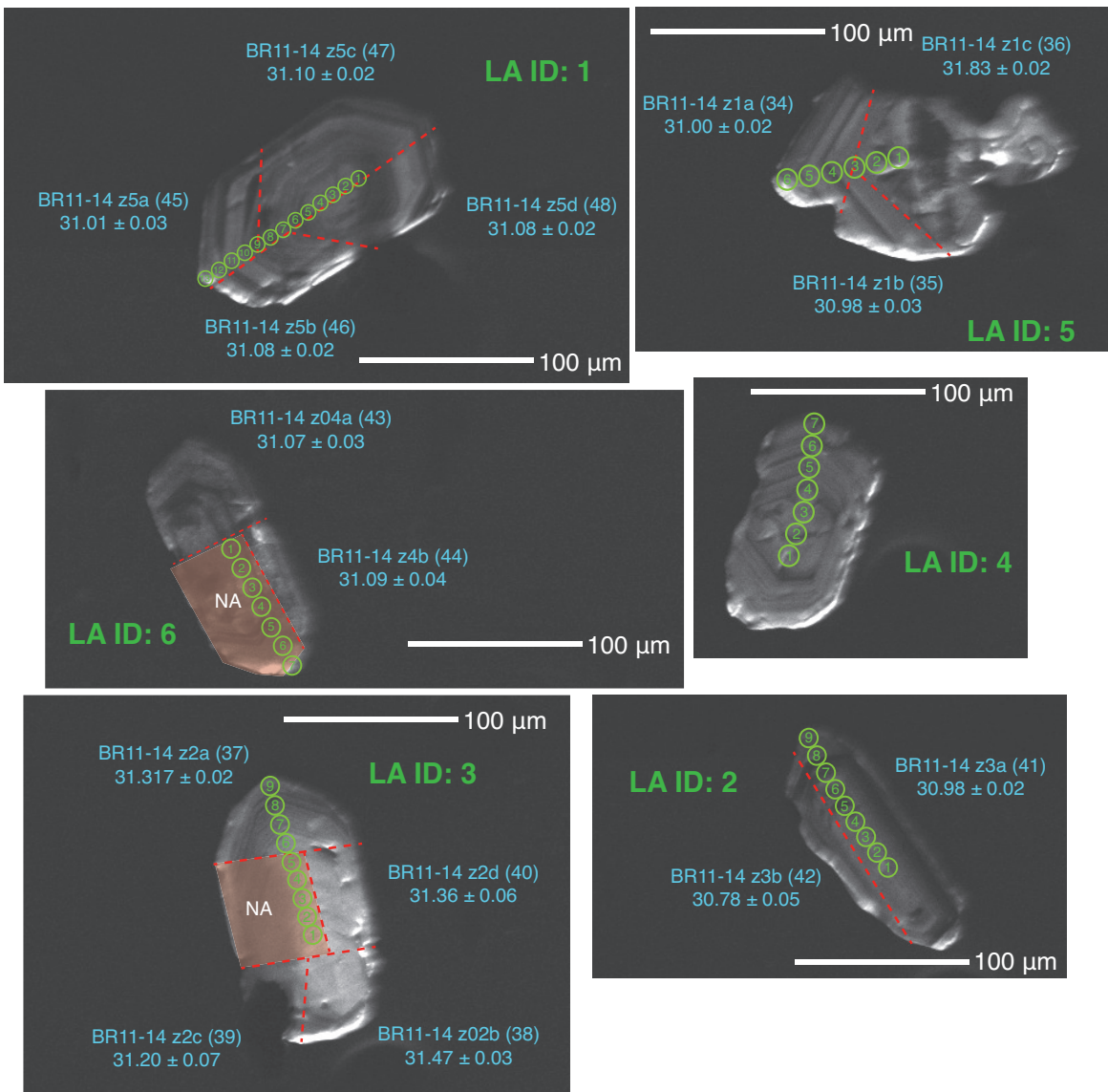


Figure DR8. BR11-14 CL images with LA-ICPMS transect points (green numbers+circles), EPMA points (blue numbers+circles), and U-Pb TIMS-TEA fragment boundaries (dashed red lines). U-Pb TIMS-TEA grain/fragment IDs+dates correspond to data in Table DR3. 15 U-Pb TIMS-TEA analyses, 51 LA-ICPMS points/6 transects/6 grains. Images and data reproduced from Samperton et al. (2015).

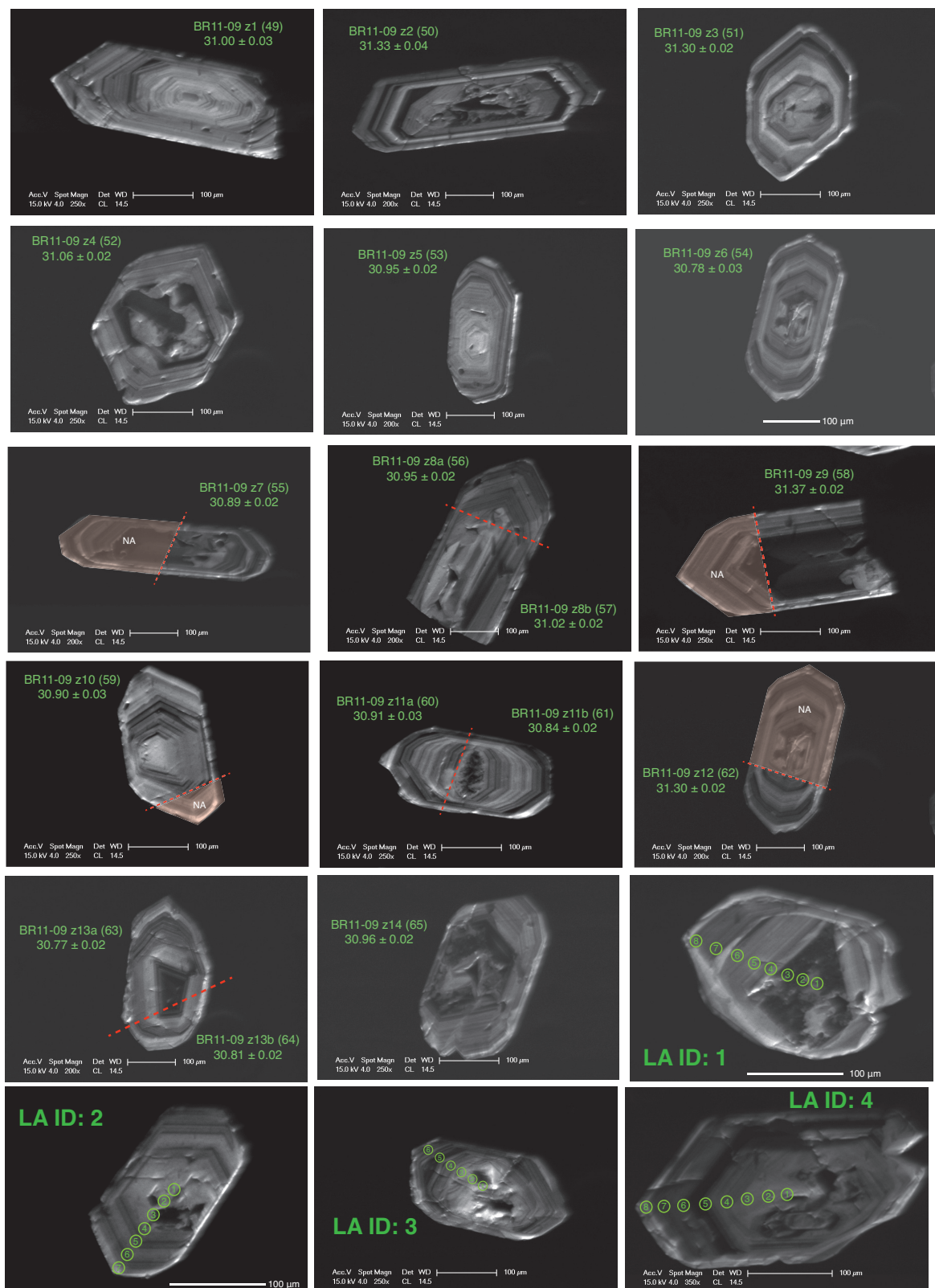


Figure DR9. BR11-09 CL images with LA-ICPMS transect points (green numbers+circles), EPMA points (blue numbers+circles), and U-Pb TIMS-TEA fragment boundaries (dashed red lines). U-Pb TIMS-TEA grain/fragment IDs+dates correspond to data in Table DR3. 17 U-Pb TIMS-TEA analyses, 29 LA-ICPMS points/4 transects/4 grains. Images and data reproduced from Samperton *et al.* (2015).

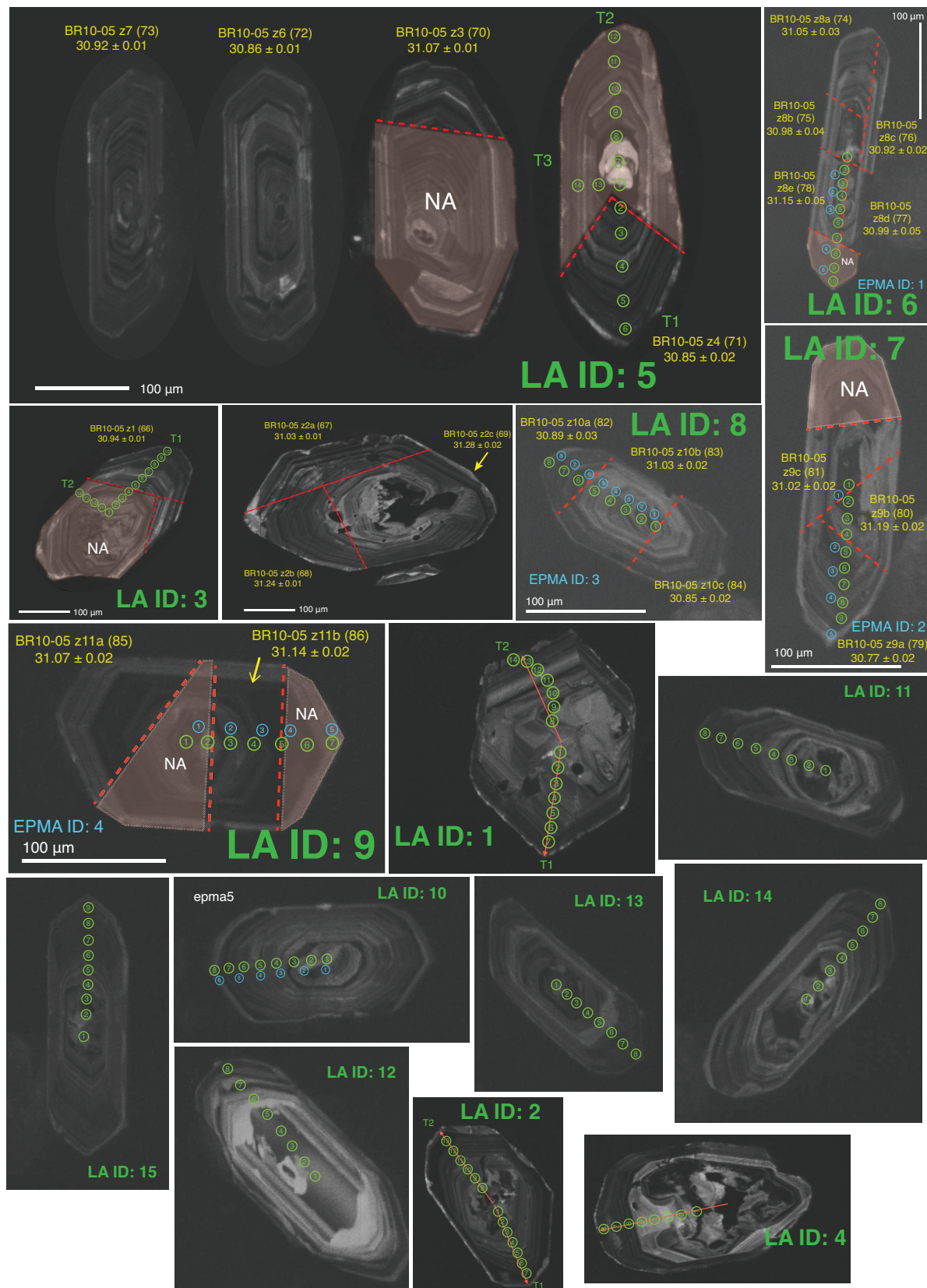


Figure DR10. BR10-05 CL images with LA-ICPMS transect points (green numbers+circles), EPMA points (blue numbers+circles), and U-Pb TIMS-TEA fragment boundaries (dashed red lines). U-Pb TIMS-TEA grain/fragment IDs+dates correspond to data in Table DR3. 21 U-Pb TIMS-TEA analyses, 149 LA-ICPMS points/20 transects/15 grains. Images and data reproduced from Samperton et al. (2015).

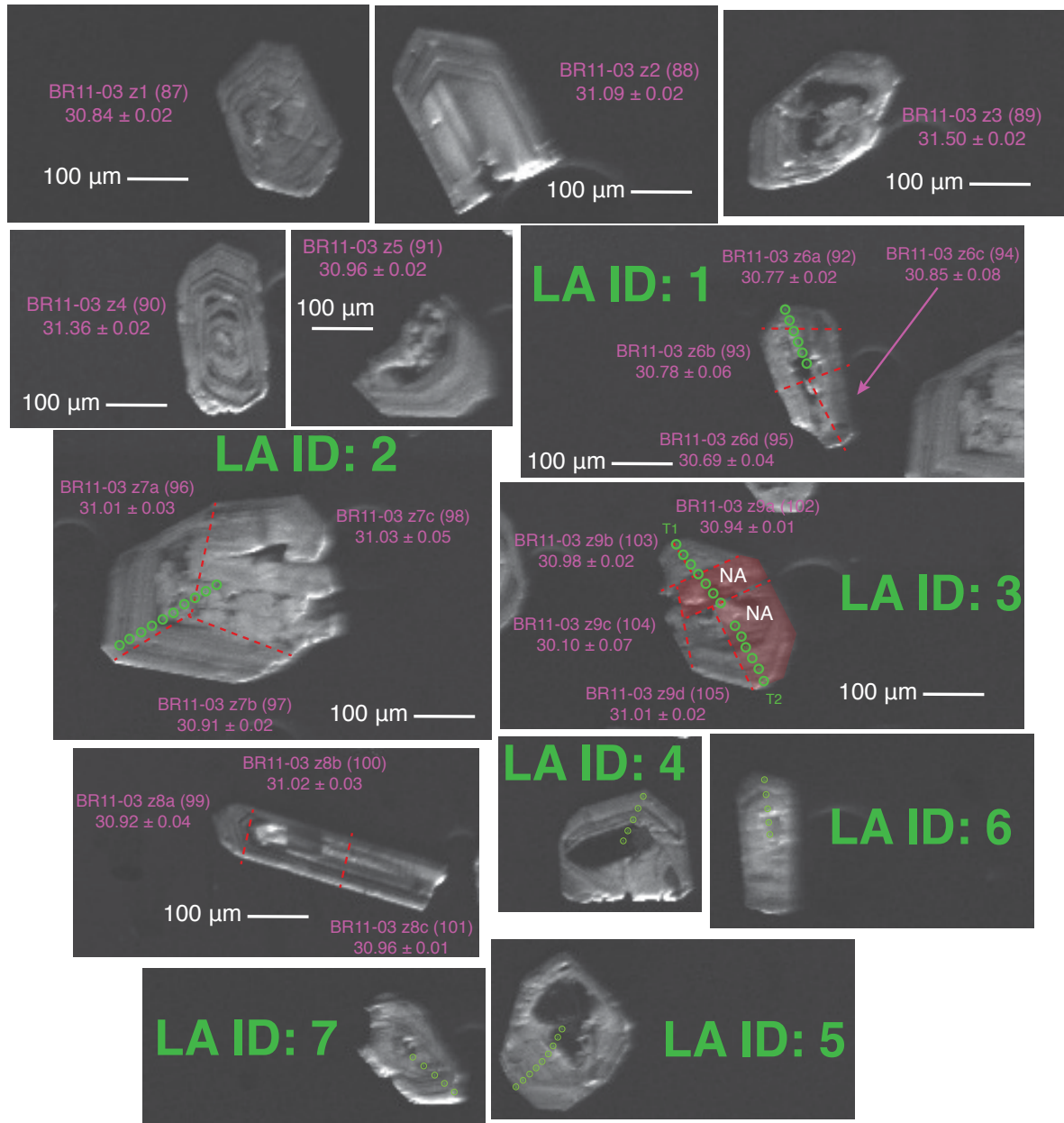


Figure DR11. BR11-03 CL images with LA-ICPMS transect points (green numbers+circles), EPMA points (blue numbers+circles), and U-Pb TIMS-TEA fragment boundaries (dashed red lines). U-Pb TIMS-TEA grain/fragment IDs+dates correspond to data in Table DR3. 19 U-Pb TIMS-TEA analyses, 53 LA-ICPMS points/8 transects/7 grains. Images and data reproduced from Samperton et al. (2015).

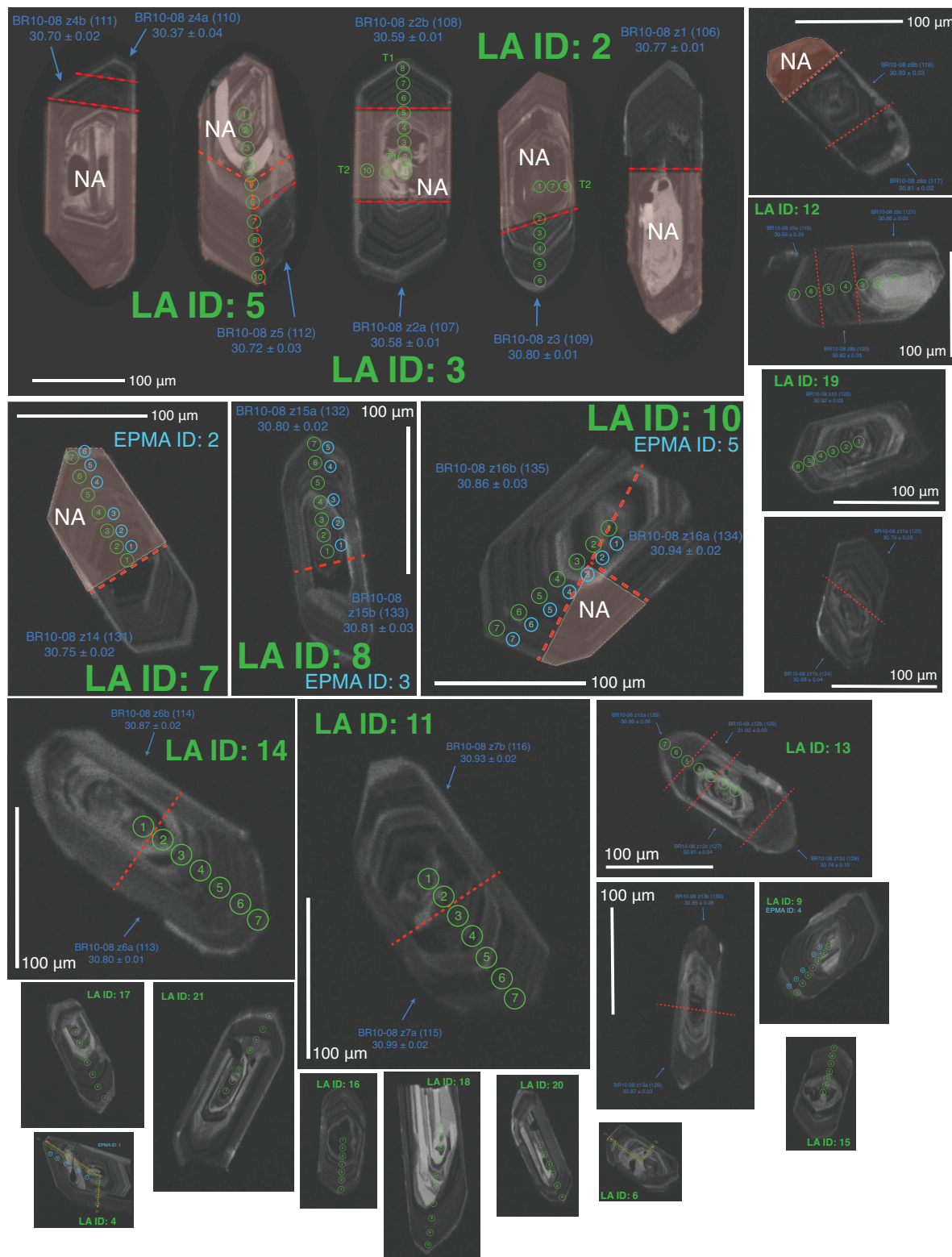


Figure DR12. BR10-08 CL images with LA-ICPMS transect points (green numbers+circles), EPMA points (blue numbers+circles), and U-Pb TIMS-TEA fragment boundaries (dashed red lines). U-Pb TIMS-TEA grain/fragment IDs+dates correspond to data in Table DR3. 30 U-Pb TIMS-TEA analyses, 163 LA-ICPMS points/24 transects/20 grains. Images and data reproduced from Samperton et al. (2015).

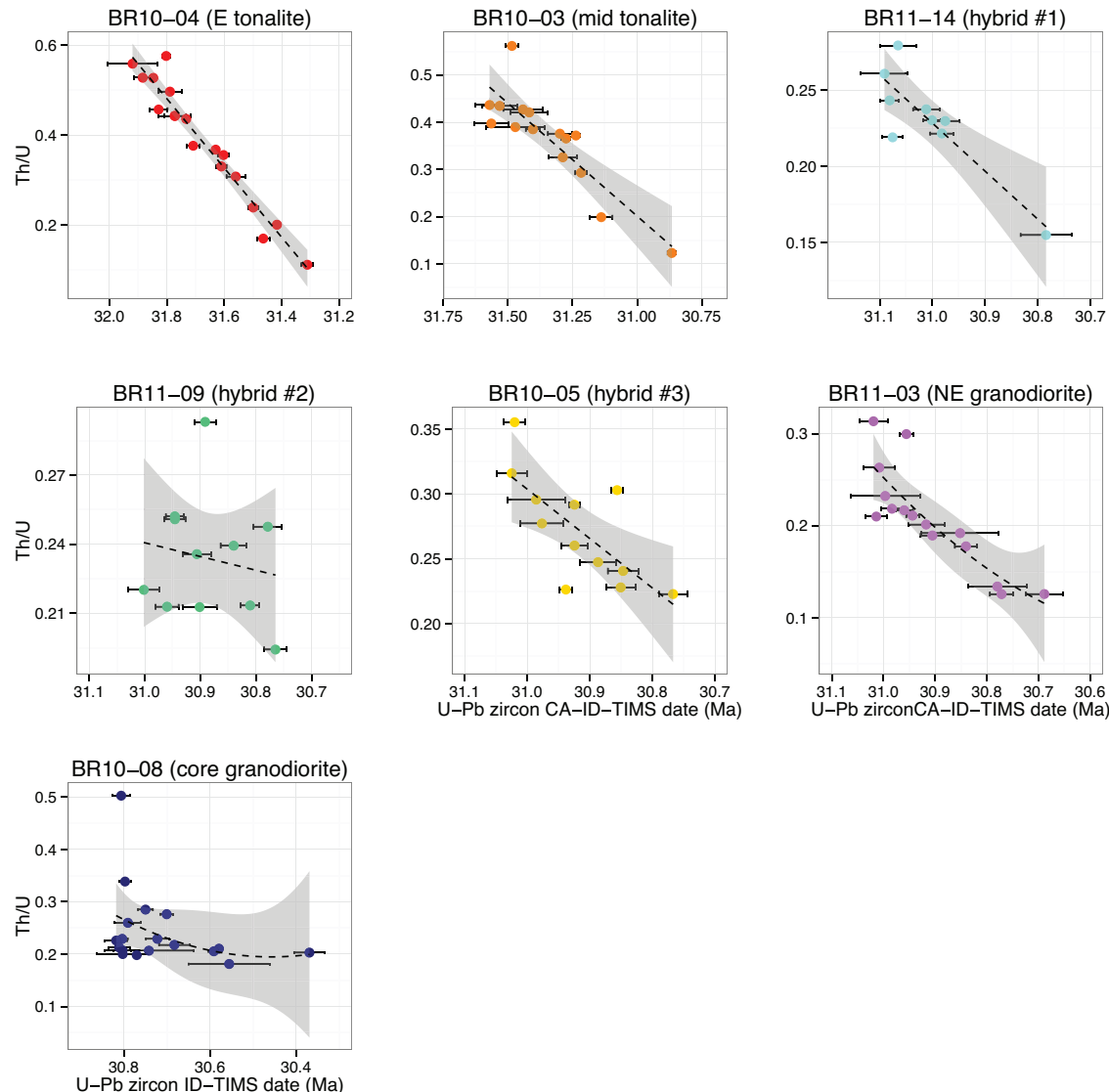


Figure DR13. Compilation of zircon Th/U vs. U-Pb CA-ID-TIMS date (Ma) for primary magmatic domains interpreted by Samperton *et al.* (2015) demonstrating strongly- to moderately-decreasing Th/U with time.

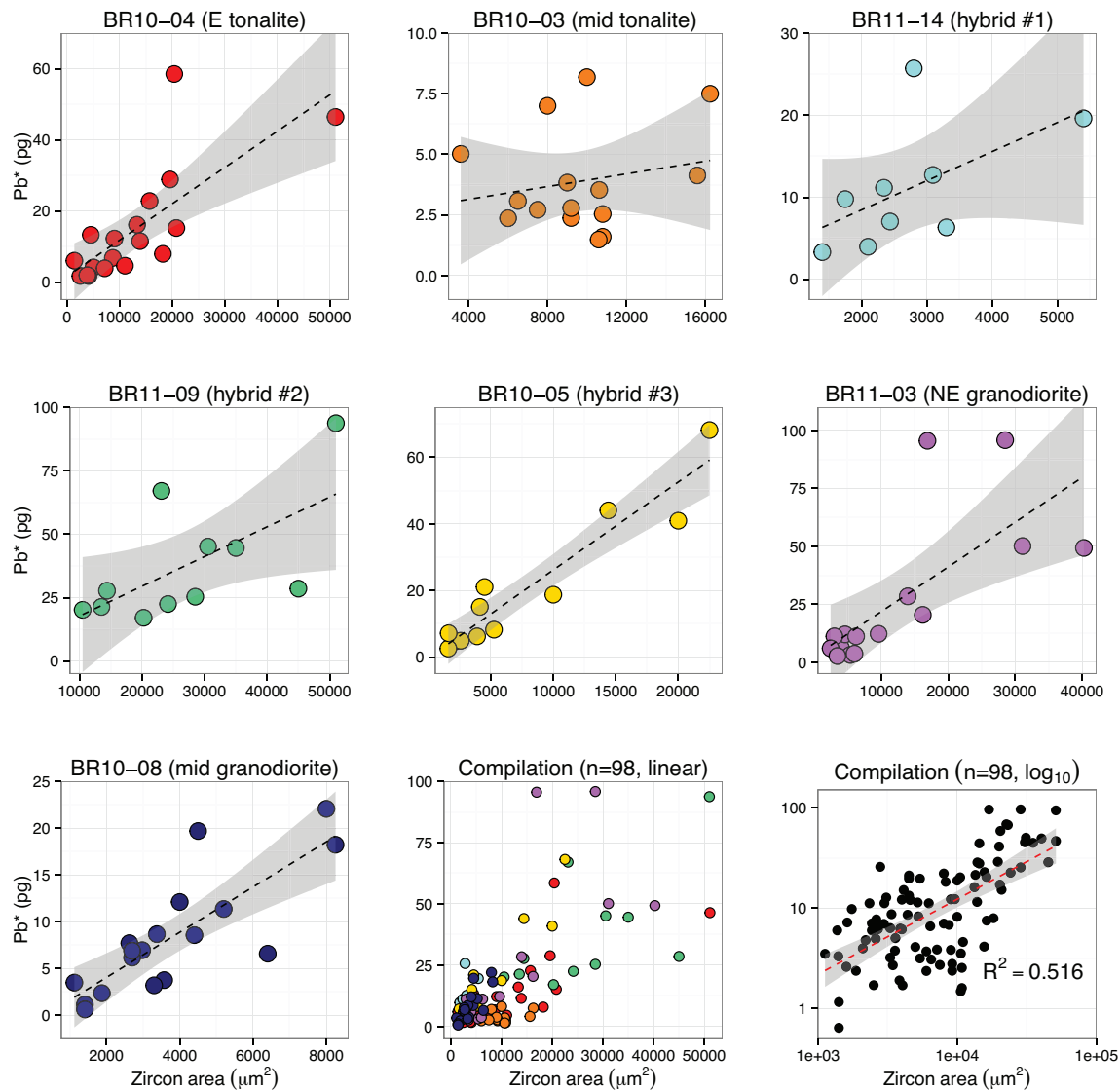


Figure DR14. Compilation of zircon radiogenic Pb (Pb^* , unit: pg) vs. grain size (unit: μm^2) for primary magmatic zircon domains interpreted by Samperton *et al.* (2015), demonstrating consistent first-order positive correlation.

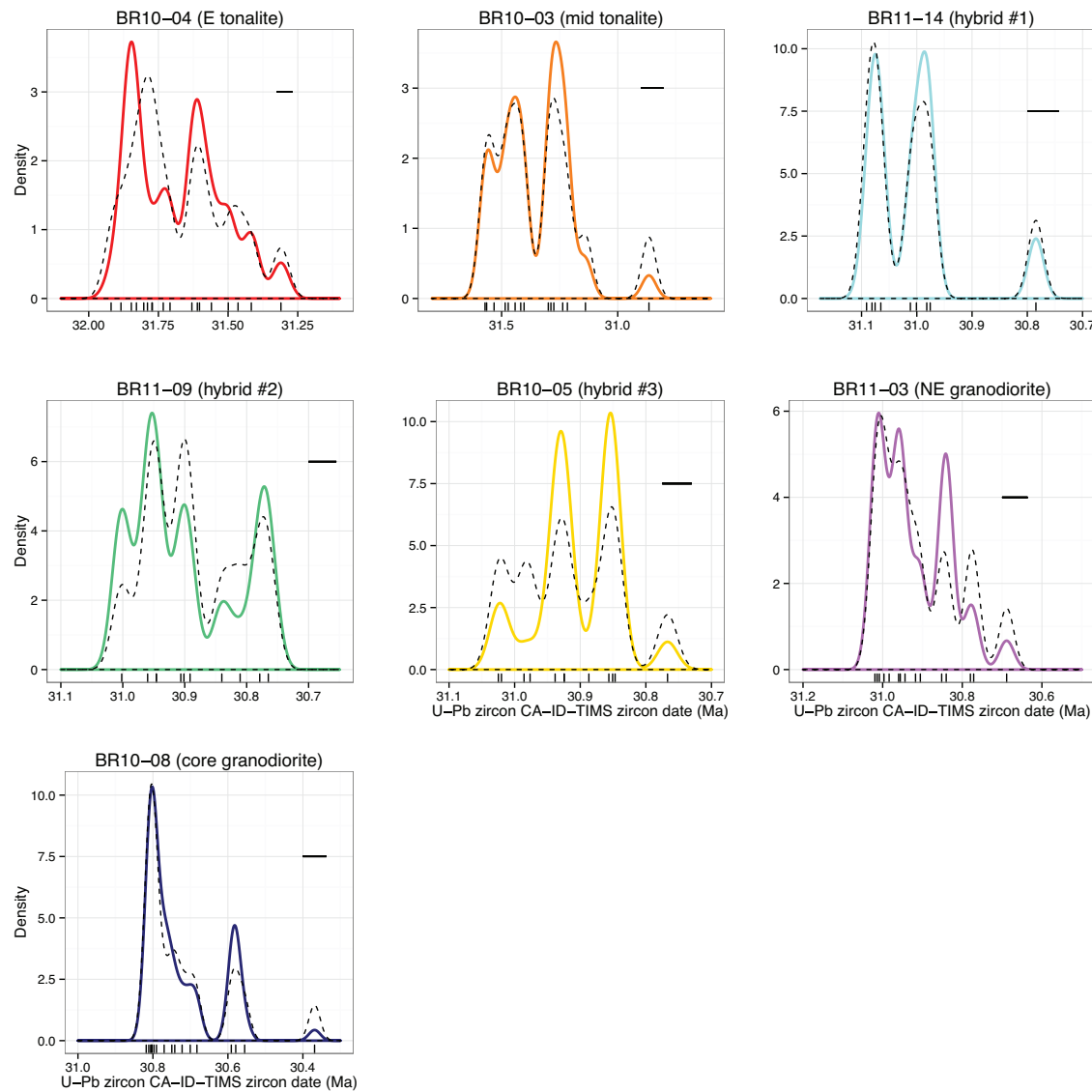


Figure DR15. Kernel density estimates (KDEs) of primary magmatic U-Pb zircon CA-ID-TIMS dates characterized by Samperton *et al.* (2015). Colored lines are mass-weighted KDEs (see description above), and dotted black lines are unweighted KDEs. Horizontal black bars indicate mean 2σ analytical uncertainties for each sample.

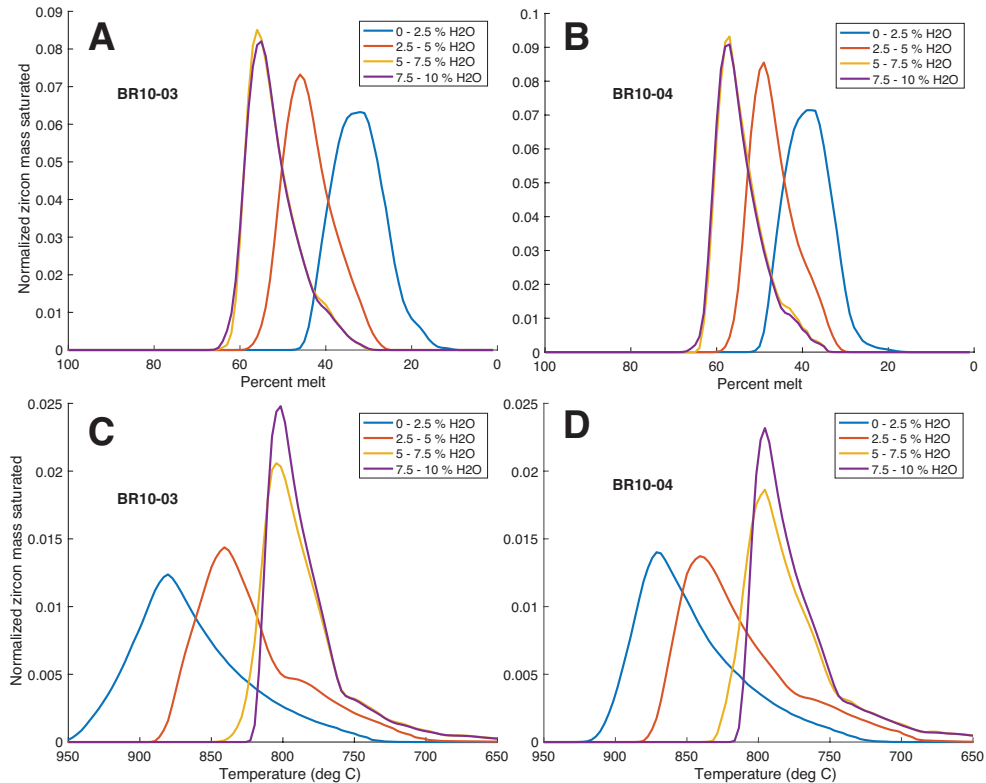


Figure DR16. Results of MELTS batch-crystallization simulations and zircon saturation modeling to produce model zircon crystallization spectra. Normalized mass of zircon saturated is plotted as a function of percent melt (A,C) and temperature (B,D) for magmatic H_2O content ranging 0–10 wt. %.

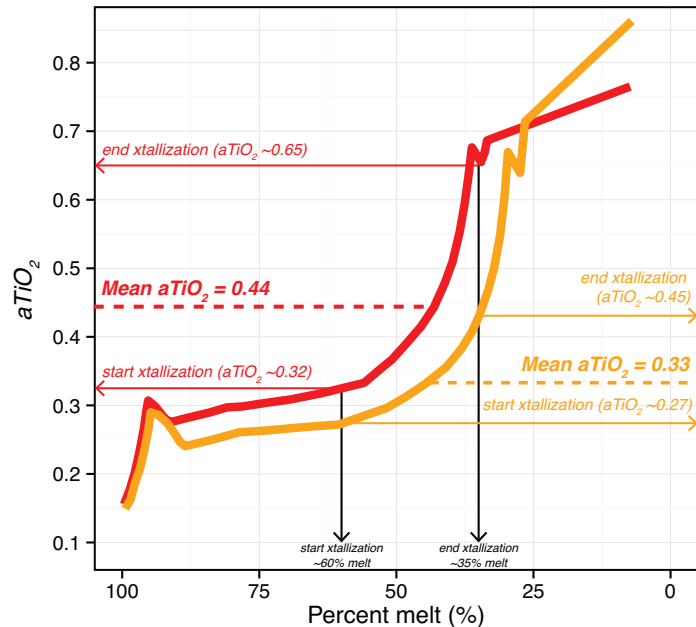


Figure DR17. $a\text{TiO}_2$ evolution as a function of % melt for water-saturated MELTS batch-crystallization simulations. The majority of zircon crystallization in hydrous simulations (>2.5 wt.% H_2O , representative of Periadriatic Intrusions, e.g., Hürlimann *et al.* (2016)) occurs between 60–35 % melt. Mean $a\text{TiO}_2$ values of 0.44 (BR10-04) and 0.33 (−03) are calculated and used for determining absolute Ti-in-zircon temperatures.

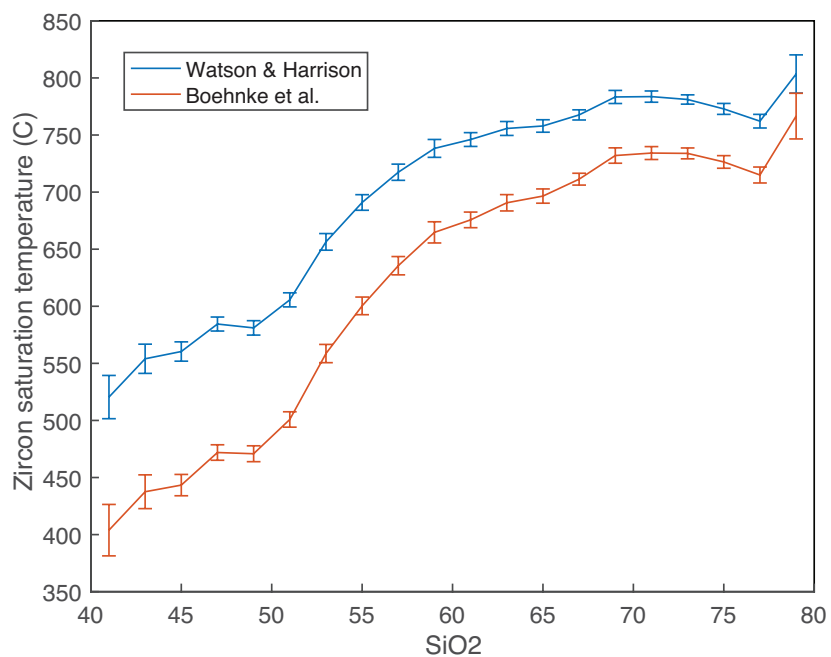


Figure DR18. Results of zircon solubility models of Watson and Harrison (1983) and Boehnke et al. (2013) used to calculate zircon saturation temperatures on database of volcanic whole-rock geochemistry, using dynamic MELTS-based approach described in the current study. Note systematic +50–70 °C bias of W&H relative to Boehnke et al.

TABLE DR1. SIMS geochemical analyses of Bergell zircons (RAW DATA)

#	Sample	Spot #	Concentration	La	Ce	Pr	Nd	Sm	Eu	Gd	Tb	Dy	Ho	Er	Tm	Yb	Lu	Y	Mg	P	Hf	Th	U	Ti (uncorrected)
1	BR10-04	s1	ppm	0.0742	14.98	0.1791	2.514	5.924	1.009	26.03	9.518	109.37	43.06	185.15	38.45	361.19	77.47	1327.0	2.12	397.9	10067	160.0	278.0	11.80
			±1sig	0.0214	0.54	0.0338	0.354	0.564	0.118	1.55	0.559	6.70	2.07	9.13	2.60	23.13	6.31	39.6	0.69	19.9	652	14.8	23.2	0.77
2	BR10-04	s2	ppm	0.0436	21.29	0.1051	1.653	3.213	0.585	22.38	8.679	112.43	44.90	194.87	43.51	396.28	95.49	1459.3	1.33	363.3	11209	196.3	353.0	8.89
			±1sig	0.0162	0.67	0.0260	0.491	0.669	0.085	1.36	0.674	7.05	2.15	8.95	4.05	26.31	7.61	41.2	0.75	18.2	737	13.2	25.8	0.65
3	BR10-04	s3	ppm	0.0647	12.40	0.1339	2.027	4.108	0.761	21.13	7.485	86.37	36.51	156.72	31.36	301.33	66.46	1086.5	2.00	310.5	10424	130.7	230.8	9.82
			±1sig	0.0199	0.48	0.0290	0.315	0.447	0.108	1.30	0.538	5.55	2.11	9.11	2.30	17.39	3.89	34.4	0.70	15.7	656	8.5	15.7	0.70
4	BR10-04	s4	ppm	0.1192	18.14	0.1961	3.703	6.317	1.081	33.35	12.068	140.03	55.74	240.13	51.45	450.98	110.38	1721.0	2.19	338.1	10495	229.9	388.0	10.11
			±1sig	0.0303	0.75	0.0356	0.663	0.726	0.167	1.97	0.715	8.46	2.62	10.89	4.34	26.17	6.32	49.4	0.46	17.0	658	17.0	30.7	0.71
5	BR10-04	s5	ppm	0.0690	16.38	0.0829	0.729	1.835	0.309	10.16	4.512	57.75	23.63	114.08	27.61	232.97	57.74	808.5	1.76	318.0	10995	123.2	261.7	10.87
			±1sig	0.0207	0.57	0.0320	0.185	0.295	0.061	0.73	0.310	3.81	1.23	5.55	1.96	13.65	3.41	28.5	0.40	16.1	682	8.1	20.6	0.74
6	BR10-04	s6	ppm	0.0447	19.77	0.1644	2.309	5.009	1.085	27.80	10.771	129.30	53.27	218.71	45.87	398.58	93.51	1541.9	1.86	318.3	11137	206.7	382.2	8.08
			±1sig	0.0166	0.65	0.0329	0.339	0.507	0.123	2.32	0.833	7.85	2.52	10.00	3.07	23.39	5.39	43.6	0.73	16.1	693	13.3	32.4	0.63
7	BR10-04	s7	ppm	0.0616	18.14	0.1407	2.979	7.175	1.117	30.30	11.874	132.88	53.37	227.41	47.48	430.16	96.73	1641.3	1.31	312.0	10424	198.6	338.4	10.75
			±1sig	0.0195	0.61	0.0302	0.462	0.641	0.125	2.21	0.678	8.81	2.52	11.51	3.37	30.70	5.88	46.7	0.28	15.8	678	14.7	22.2	0.73
8	BR10-04	s8	ppm	0.1036	17.08	0.2043	3.581	6.667	1.224	31.00	11.565	131.34	53.15	218.44	49.52	430.15	96.90	1610.7	2.68	303.1	10138	203.6	326.8	10.98
			±1sig	0.0332	0.58	0.0361	0.429	0.866	0.131	1.80	0.661	7.96	2.51	9.96	3.56	24.41	5.71	46.5	0.73	15.4	628	13.0	25.9	0.73
9	BR10-04	s9	ppm	0.0869	15.44	0.1695	2.537	4.559	1.127	23.35	9.276	108.35	44.46	189.64	41.57	361.46	83.98	1327.5	2.28	311.6	9852	164.7	312.2	11.10
			±1sig	0.0459	0.55	0.0332	0.507	0.481	0.208	1.70	0.590	8.58	2.56	8.77	3.19	23.68	4.87	37.9	0.38	15.8	609	10.6	20.6	0.76
10	BR10-04	s10	ppm	0.0897	24.92	0.0592	1.052	2.229	0.610	21.14	8.998	120.61	49.43	219.56	47.81	438.54	96.57	1535.6	2.14	306.8	11637	215.8	382.2	6.63
			±1sig	0.0233	0.75	0.0209	0.324	0.311	0.103	1.30	0.673	7.47	2.35	10.01	3.19	24.87	6.08	48.6	0.54	15.5	750	24.7	25.0	0.56
11	BR10-04	s11	ppm	0.0864	12.75	0.0711	1.151	2.032	0.486	15.69	6.112	76.15	34.70	147.00	35.02	312.69	75.28	1014.7	1.80	464.9	10852	103.9	261.1	7.44
			±1sig	0.0231	0.49	0.0214	0.234	0.296	0.078	1.20	0.392	5.41	1.71	8.58	2.38	18.03	5.04	28.7	0.52	23.1	673	7.0	20.5	0.60
12	BR10-04	s12	ppm	0.1316	16.73	0.2008	3.589	5.498	0.921	24.78	10.758	115.87	45.75	212.45	46.19	387.50	94.90	1476.3	2.16	369.3	10495	182.2	347.2	9.82
			±1sig	0.0285	0.58	0.0361	0.433	0.538	0.133	1.56	0.622	7.55	2.19	10.13	3.09	32.11	6.52	42.8	0.76	18.5	790	11.7	28.4	0.70
13	BR10-04	s13	ppm	0.0577	16.15	0.1089	2.744	5.143	1.062	25.30	10.061	114.99	43.81	208.71	43.39	382.33	93.02	1434.7	1.76	332.5	10138	173.3	306.3	10.05
			±1sig	0.0180	0.89	0.0457	0.358	0.500	0.117	1.50	0.580	6.99	2.16	9.70	2.90	23.30	5.34	43.4	0.56	16.7	640	11.1	22.0	0.68
14	BR10-04	s14	ppm	0.0567	13.10	0.0738	0.785	2.006	0.378	12.04	5.389	70.53	31.80	144.00	35.03	302.24	71.75	963.2	1.58	457.4	11209	102.3	248.0	8.78
			±1sig	0.0187	0.49	0.0218	0.191	0.406	0.068	0.82	0.409	6.14	1.58	6.82	2.47	21.28	6.86	29.2	0.31	22.8	755	8.5	19.9	0.65
15	BR10-04	s15	ppm	0.0776	12.40	0.0711	0.724	1.479	0.318	12.47	4.886	64.91	28.15	128.67	29.55	273.16	62.54	865.3	1.36	431.4	10995	85.6	235.2	9.30
			±1sig	0.0220	0.48	0.0214	0.185	0.249	0.075	1.12	0.405	4.12	1.44	6.17	2.03	16.77	3.68	30.2	0.47	21.5	730	8.3	28.4	0.68
16	BR10-04	s16	ppm	0.0791	13.81	0.0472	0.952	1.943	0.423	11.54	5.065	63.87	28.68	134.28	30.08	290.34	69.98	902.8	2.05	379.3	11352	104.7	257.3	9.53
			±1sig	0.0226	0.52	0.0184	0.275	0.348	0.141	0.81	0.335	4.05	1.46	7.46	2.07	16.82	4.19	25.7	0.51	19.1	708	10.0	17.1	0.70
17	BR10-04	s17	ppm	0.0907	18.95	0.1013	2.354	5.321	1.161	26.82	11.073	130.83	50.48	207.59	45.00	389.01	84.23	1526.1	1.72	283.4	10566	188.7	294.7	8.95
			±1sig	0.0235	0.63	0.0257	0.341	0.525	0.135	1.59	0.637	7.93	3.14	15.52	3.01	26.36	5.25	51.3	0.30	14.4	710	12.7	26.6	0.66
18	BR10-04	s18	ppm	0.1368	14.27	0.0826	1.509	3.117	0.481	14.91	6.552	74.62	32.87	151.11	30.72	292.28	75.65	1085.8	1.74	446.3	10566	114.6	238.1	10.05
			±1sig	0.0293	0.52	0.0232	0.271	0.542	0.145	1.02	0.204	8.00	2.46	8.24	2.38	17.33	5.25	36.0	0.45	22.2	781	7.5	16.1	0.74
19	BR10-04	s19	ppm	0.1109	17.43	0.2973	4.922	7.302	1.104	30.12	11.148	133.39	51.21	233.40	51.99	459.84	104.67	1635.8	1.32	328.4	10067	219.0	431.8	9.59
			±1sig	0.0263	0.71	0.0448	0.521	0.674	0.125	1.77	0.643	8.09	2.43	10.64	3.46	26.61	7.08	48.7	0.29	16.6	644	17.0	28.2	0.69
20	BR10-04	s20	ppm	0.0103	2.13	0.0053	bdi	0.190	0.022	0.28	0.200	2.36	1.48	6.66	2.50	30.03	8.99	44.8	1.60	59.1	6176	27.7	217.9	2.75
			±1sig	0.0063	0.14	0.0053	bdi	0.068	0.012	0.01	0.010	0.29	0.15	0.98	0.56	2.00	1.00	1.4	0.47	3.4	395	2.0	14.5	0.29
21	BR10-04	s21	ppm	0.0384	11.40	0.0394	0.286	0.737	0.254	6.18	2.943	34.70	15.15	74.81	17.19	162.78	41.86	494.5	1.42	219.8	12351	75.2	225.5	7.15
			±1sig	0.0157	0.53	0.0167	0.116	0.293	0.056	0.57	0.222	3.50	1.34	4.23	1.41	9.84	2.80	16.9	0.30	12.7	763	5.3	16.3	0.60
22	BR10-04	s22	ppm	0.0855	14.51	0.0621	1.021	2.927	0.517	17.40	6.809	87.39	35.66	151.04	33.22	220.2	74.74	274.7	4.91	296.8	10424	247.8	585.3	6.88
			±1sig	0.0231	0.53	0.0205	0.222	0.455	0.081	0.91	0.277	3.59	1.25	8.31	2.04	17.08	6.23	20.9	0.98	15.3	652	21.2	39.6	0.64
23	BR10-04	s23	ppm	0.0923	12.99	0.0965	0.960	2.863	0.416	12.17	5.569	59.28	26.20	120.44	26.64	263.52	64.55	819.7	2.69	298.3	10780	136.5	297.6	11.27
			±1sig	0.0414	0.89	0.0264	0.305	0.380	0.076	1.19	0.367	6.28	1.36	9.41	2.48	15.50	5.92	28.3	0.78	15.7	745	10.7	31.8	0.80
24	BR10-0																							

23	BR10-03	s23	<i>ppm</i>	0.0680	14.58	0.0885	0.667	1.345	0.461	7.59	3.581	39.82	19.07	99.12	24.68	261.18	75.91	654.7	2.31	184.3	10616	268.0	555.2	5.99
			$\pm 1\sigma$	0.0165	0.67	0.0195	0.143	0.239	0.064	0.53	0.230	2.54	0.96	6.19	1.90	14.85	7.39	20.5	0.36	9.4	1083	30.8	40.6	0.44
1	BR11-03	s1	<i>ppm</i>	0.0597	45.40	0.0932	1.170	3.018	0.797	20.38	9.974	118.82	55.06	258.50	61.39	595.18	129.33	1655.5	1.41	320.8	12837	696.8	2912.0	3.79
			$\pm 1\sigma$	0.0145	1.05	0.0208	0.181	0.299	0.082	1.60	0.547	7.51	5.15	29.00	8.02	107.78	14.84	52.9	0.33	17.7	2168	58.4	194.4	0.32
2	BR11-03	s2	<i>ppm</i>	0.0994	31.30	0.2018	2.857	4.135	0.756	25.47	12.077	143.40	61.71	291.22	64.09	598.65	150.84	2087.4	1.49	414.3	11252	533.4	1189.8	12.73
			$\pm 1\sigma$	0.0194	0.79	0.0299	0.555	0.376	0.137	1.46	0.812	10.31	2.80	12.87	4.17	37.80	8.47	59.2	0.24	20.3	705	36.6	89.4	0.65
3	BR11-03	s3	<i>ppm</i>	0.0844	10.35	0.1463	1.727	2.114	0.520	12.58	4.247	50.16	20.77	97.88	22.87	217.64	51.10	686.4	1.45	265.4	11038	144.1	410.8	11.97
			$\pm 1\sigma$	0.0179	0.36	0.0242	0.232	0.258	0.131	0.78	0.262	3.33	1.03	4.77	1.81	14.10	4.11	20.0	0.40	13.2	935	9.1	26.6	0.62
4	BR11-03	s4	<i>ppm</i>	0.2947	146.25	0.4223	7.166	15.511	4.811	81.46	32.725	402.26	170.14	765.65	174.96	1658.81	380.62	5536.3	9.05	808.1	8860	2032.2	4064.1	14.54
			$\pm 1\sigma$	0.0328	3.80	0.0486	0.979	1.083	0.565	5.26	1.688	40.82	13.83	58.27	16.33	175.04	30.42	155.7	0.59	39.1	722	161.9	338.5	3.59
5	BR11-03	s5	<i>ppm</i>	0.1232	41.21	0.0730	1.137	2.739	0.699	18.56	9.256	122.30	55.94	270.65	65.52	644.89	158.41	1755.0	1.22	232.0	13508	570.0	3261.8	2.69
			$\pm 1\sigma$	0.0327	0.99	0.0190	0.248	0.286	0.077	1.20	0.528	7.29	2.55	11.93	4.35	35.74	8.88	60.2	0.29	11.6	852	41.7	250.5	0.28
6	BR11-03	s6	<i>ppm</i>	0.0723	48.93	0.0548	0.812	2.950	0.799	24.36	11.573	158.63	70.99	333.86	83.91	824.21	192.45	2370.7	0.88	219.7	13037	883.7	4501.8	2.47
			$\pm 1\sigma$	0.0165	2.37	0.0181	0.155	0.303	0.084	2.47	0.720	9.39	3.37	14.96	5.87	62.92	15.25	137.9	0.46	11.0	804	66.4	286.7	0.27
7	BR11-03	s7	<i>ppm</i>	0.0881	36.50	0.1326	1.981	4.457	1.091	23.20	9.312	109.37	46.51	220.31	50.59	467.37	113.80	1488.1	1.28	245.8	11994	535.0	1753.4	2.14
			$\pm 1\sigma$	0.0184	0.89	0.0247	0.370	0.398	0.145	1.33	0.519	6.97	2.21	9.77	3.31	26.09	6.79	65.8	0.39	12.9	760	36.7	183.5	0.25
8	BR11-03	s8	<i>ppm</i>	0.1649	46.84	0.1128	1.311	4.178	1.068	25.61	12.012	151.73	62.78	299.83	71.10	685.17	160.52	2056.4	1.19	213.1	12829	742.2	2790.9	3.76
			$\pm 1\sigma$	0.0543	1.08	0.0230	0.269	0.559	0.099	1.79	1.135	9.06	3.09	17.63	5.39	37.97	9.26	76.8	2.45	11.6	803	47.6	182.7	0.35
9	BR11-03	s9	<i>ppm</i>	0.0513	57.97	0.2038	4.500	7.867	1.830	31.37	12.928	144.68	58.59	276.15	62.79	563.67	130.19	1995.0	1.05	273.9	11709	655.1	1921.8	2.19
			$\pm 1\sigma$	0.0142	2.28	0.0317	0.410	0.596	0.179	2.26	0.805	18.87	3.54	23.51	5.37	56.46	9.97	128.6	0.53	13.6	731	91.6	156.9	0.26
10	BR11-03	s10	<i>ppm</i>	0.2986	36.63	0.1054	1.407	2.707	0.593	18.08	8.694	120.87	53.71	265.30	64.95	637.54	144.92	1800.6	2.79	225.1	13144	691.6	4186.7	5.56
			$\pm 1\sigma$	0.0333	1.45	0.0218	0.205	0.284	0.115	1.52	0.485	11.31	2.77	11.64	4.49	46.79	8.98	70.2	11.84	11.5	811	45.2	269.1	0.40
11	BR11-03	s11	<i>ppm</i>	0.0538	30.23	0.0803	0.659	2.222	0.589	17.42	8.123	107.78	47.02	230.55	55.11	546.63	131.12	1557.5	1.08	279.3	14507	616.4	2817.8	1.90
			$\pm 1\sigma$	0.0152	1.55	0.0204	0.147	0.327	0.074	1.12	0.648	11.52	5.10	10.25	4.18	52.49	8.45	85.1	0.22	14.0	895	53.0	180.8	0.25
12	BR11-03	s12	<i>ppm</i>	0.1613	38.88	0.2044	4.236	10.155	1.435	70.87	29.617	351.46	142.88	586.11	126.88	1168.55	252.47	4384.3	2.43	989.6	12401	1239.9	2620.0	4.58
			$\pm 1\sigma$	0.0243	2.76	0.0499	0.636	1.226	0.159	4.39	1.616	25.81	8.96	49.52	10.39	170.92	22.73	174.6	0.30	47.8	1160	142.4	255.6	0.36
13	BR11-03	s13	<i>ppm</i>	0.1371	17.39	0.2870	4.509	11.257	1.547	65.09	26.800	330.25	133.20	575.26	127.96	1117.32	256.85	4095.7	2.89	1169.2	12530	607.3	1600.3	5.06
			$\pm 1\sigma$	0.0241	0.52	0.0373	0.423	0.795	0.133	6.42	2.852	36.30	17.02	54.25	11.95	115.79	30.86	185.3	0.38	72.4	773	119.6	264.8	0.41
14	BR11-03	s14	<i>ppm</i>	0.1229	35.91	0.0250	0.770	2.130	0.767	15.33	7.257	91.12	40.41	194.57	46.78	455.40	111.65	1227.6	4.67	173.4	13536	513.1	2143.2	17.13
			$\pm 1\sigma$	0.0291	1.07	0.0126	0.184	0.285	0.078	0.97	0.408	7.57	1.86	12.90	3.18	28.55	6.46	34.6	1.35	8.8	983	44.8	182.4	5.32
15	BR11-03	s15	<i>ppm</i>	0.1302	37.07	0.0895	1.010	3.083	0.791	16.69	7.753	98.94	42.19	201.87	47.89	461.36	111.70	1354.3	1.23	159.8	12929	743.8	3083.8	2.28
			$\pm 1\sigma$	0.0209	1.04	0.0195	0.164	0.297	0.122	0.98	0.528	5.93	3.55	14.78	3.24	25.97	6.29	43.2	0.20	8.1	798	45.9	205.6	0.24
16	BR11-03	s16	<i>ppm</i>	0.0707	58.71	0.0216	1.433	3.581	1.022	23.18	10.276	129.55	54.50	271.85	63.54	610.27	139.54	1756.8	1.97	205.7	13579	969.0	3504.0	2.74
			$\pm 1\sigma$	0.0161	1.36	0.0325	0.253	0.587	0.097	2.29	0.565	7.71	2.54	15.49	4.39	36.34	8.07	70.4	0.27	10.4	838	85.8	222.6	0.28
17	BR11-03	s17	<i>ppm</i>	0.1524	246.05	0.6278	12.641	22.152	8.490	121.99	47.499	538.66	232.65	1046.92	218.52	1858.57	410.67	6977.6	2.26	525.1	8203	5391.8	5129.0	13.40
			$\pm 1\sigma$	0.0231	5.46	0.0630	0.795	1.341	0.475	6.57	2.425	35.38	11.63	45.17	21.55	156.78	32.76	271.8	0.29	26.9	603	347.1	328.8	0.64
18	BR11-03	s18	<i>ppm</i>	0.0937	49.46	0.0156	1.232	4.105	0.958	22.87	11.196	131.29	54.92	267.14	63.36	617.13	146.36	1745.0	12.87	186.2	15721	1404.6	5242.8	19.75
			$\pm 1\sigma$	0.0210	1.86	0.0125	0.177	0.353	0.088	2.75	0.967	14.62	7.58	43.52	8.62	49.09	10.57	90.6	3.12	9.3	974	86.4	469.8	3.37
19	BR11-03	s19	<i>ppm</i>	0.0831	47.78	0.0408	1.509	3.427	0.859	21.22	9.828	132.31	56.59	278.28	64.23	637.22	153.25	1860.5	17.75	236.1	12523	632.1	2580.9	7.68
			$\pm 1\sigma$	0.0167	2.98	0.0157	0.205	0.320	0.203	1.31	0.615	12.03	3.54	20.02	5.56	42.62	9.60	74.3	0.87	12.4	971	48.2	167.2	0.47
20	BR11-03	s20	<i>ppm</i>	0.0592	78.34	0.1590	3.804	7.409	2.048	37.68	14.630	174.73	70.93	320.58	73.52	682.26	156.84	2114.2	2.81	261.7	11444	1691.1	3153.9	3.48
			$\pm 1\sigma$	0.0146	3.00	0.0283	0.359	0.558	0.156	2.07	0.782	12.96	3.77	13.97	5.26	37.99	9.62	74.1	0.84	14.9	710	142.8	245.0	0.31
21	BR11-03	s21	<i>ppm</i>	0.0623	52.95	0.0857	1.186	3.147	0.953	15.28	7.045	83.25	35.98	171.79	39.16	373.94	89.79	1181.0	4.60	148.3	12665	821.3	2018.6	2.87
			$\pm 1\sigma$	0.0164	1.19	0.0207	0.184	0.451	0.092	0.92	0.514	5.03	2.08	7.68	2.93	20.94	5.16	35.3	1.04	7.6	781	54.3	145.2	0.28
22	BR11-03	s22	<i>ppm</i>	0.0916	22.14	0.0858	1.329	3.528	0.772	18.41</td														

TABLE DR2. SIMS Ti-in-zircon thermometry (REDUCED DATA)

#	Sample	Spot #	Ti (ppm; uncorrected)	Ti (ppm; 91500-corrected)	Zr (ppm)	Th (ppm)	Zr (ppm)	U (ppm)	Zr (ppm)	Th/U	Zr	³⁹ Fe/ ⁴⁰ Si	LREE-I	aSiO ₂	aTiO ₃	Ti-in-zircon temperature (°C)	Zr (upper-limit)	Zr (lower-limit)
1	BR10-04	s1	11.80	9.10	1.54	160	30	278	46	0.575	0.143	112	62.0	1	0.44	818.9	17.1	19.7
2	BR10-04	s2	8.89	6.86	1.30	196	26	353	52	0.556	0.110	107	103.0	1	0.44	789.2	18.0	21.0
3	BR10-04	s3	9.82	7.58	1.40	131	17	231	31	0.567	0.107	114	63.6	1	0.44	799.5	17.9	20.8
4	BR10-04	s4	10.11	7.80	1.41	230	34	388	61	0.593	0.128	110	60.0	1	0.44	802.5	17.7	20.5
5	BR10-04	s5	10.87	8.38	1.49	123	16	262	41	0.471	0.096	120	110.7	1	0.44	810.1	17.6	20.3
6	BR10-04	s6	8.08	6.23	1.26	207	27	382	65	0.541	0.115	106	81.8	1	0.44	779.5	18.8	22.1
7	BR10-04	s7	10.75	8.29	1.46	199	29	338	44	0.587	0.116	110	63.1	1	0.44	809.0	17.5	20.2
8	BR10-04	s8	10.98	8.47	1.47	204	26	327	52	0.623	0.127	111	56.4	1	0.44	811.3	17.2	19.8
9	BR10-04	s9	11.10	8.56	1.52	165	21	312	41	0.528	0.097	110	66.5	1	0.44	812.4	17.7	20.5
10	BR10-04	s10	6.63	5.11	1.13	216	49	382	50	0.565	0.149	114	168.8	1	0.44	760.0	19.6	23.5
11	BR10-04	s11	7.44	5.74	1.21	104	14	261	41	0.398	0.082	105	103.7	1	0.44	771.3	19.2	22.8
12	BR10-04	s12	9.82	7.58	1.40	182	23	347	57	0.525	0.109	117	54.6	1	0.44	799.5	17.9	20.8
13	BR10-04	s13	10.05	7.76	1.35	173	22	306	44	0.566	0.109	120	64.3	1	0.44	801.9	17.1	19.7
14	BR10-04	s14	8.78	6.77	1.31	102	17	248	40	0.413	0.095	112	125.0	1	0.44	787.9	18.3	21.4
15	BR10-04	s15	9.30	7.17	1.36	86	17	235	57	0.364	0.113	119	133.5	1	0.44	793.8	18.2	21.2
16	BR10-04	s16	9.53	7.35	1.41	105	20	257	34	0.407	0.095	110	99.2	1	0.44	796.4	18.4	21.5
17	BR10-04	s17	8.95	6.90	1.32	189	25	295	53	0.640	0.144	117	80.2	1	0.44	789.9	18.2	21.3
18	BR10-04	s18	10.05	7.76	1.49	115	15	238	32	0.481	0.091	112	73.4	1	0.44	801.9	18.7	21.8
19	BR10-04	s19	9.59	7.40	1.38	219	34	432	50	0.507	0.103	108	45.4	1	0.44	797.0	18.1	21.0
20	BR10-04	s20	2.75	2.12	0.57	28	4	218	29	0.127	0.025	131	12.4	1	0.44	681.5	20.2	25.3
21	BR10-04	s21	7.15	5.51	1.20	75	11	226	33	0.333	0.067	107	168.6	1	0.44	767.4	19.7	23.6
22	BR10-04	s22	9.82	7.58	1.41	130	17	235	34	0.553	0.107	101	115.4	1	0.44	799.5	18.0	21.0
23	BR10-04	s23	11.27	8.70	1.59	136	21	298	64	0.459	0.122	107	82.5	1	0.44	814.0	18.3	21.2
24	BR10-04	s24	14.99	11.57	1.76	321	40	484	84	0.663	0.142	111	57.0	1	0.44	845.4	16.3	18.4
25	BR10-04	s25	10.29	7.94	1.44	172	25	338	44	0.508	0.101	121	74.5	1	0.44	804.3	17.8	20.6
1	BR10-03	s1	6.71	5.17	1.30	135	18	407	54	0.332	0.062	336	60.4	1	0.33	789.8	23.4	28.7
2	BR10-03	s2	6.17	4.76	1.21	452	69	731	121	0.619	0.140	143	53.1	1	0.33	781.3	23.3	28.8
3	BR10-03	s3	6.88	5.30	1.27	248	42	585	79	0.423	0.092	119	91.8	1	0.33	792.4	22.5	27.4
4	BR10-03	s4	5.91	4.56	1.18	212	28	425	63	0.498	0.100	133	100.4	1	0.33	777.0	23.5	29.0
5	BR10-03	s5	5.29	4.08	1.13	178	25	451	67	0.396	0.080	113	93.9	1	0.33	766.1	24.4	30.7
6	BR10-03	s6	6.93	5.34	1.22	721	91	1036	164	0.696	0.141	116	84.8	1	0.33	793.1	21.5	25.9
7	BR10-03	s7	6.39	4.93	1.18	565	75	926	119	0.610	0.113	113	51.6	1	0.33	784.8	22.2	27.1
8	BR10-03	s8	13.12	10.12	3.77	144	19	496	65	0.289	0.053	166	77.4	1	0.33	863.1	38.2	51.9
9	BR10-03	s9	5.10	3.93	1.03	270	45	654	92	0.413	0.091	117	92.0	1	0.33	762.5	23.2	28.8
10	BR10-03	s10	4.73	3.65	1.01	146	23	392	55	0.372	0.079	139	73.5	1	0.33	755.3	24.0	30.2
11	BR10-03	s11	7.09	5.47	2.34	137	18	526	76	0.261	0.051	197	99.6	1	0.33	795.5	38.2	54.8
12	BR10-03	s12	4.94	3.81	1.01	257	33	521	68	0.493	0.090	129	68.0	1	0.33	759.5	23.3	29.0
13	BR10-03	s13	5.17	3.99	1.02	224	39	519	69	0.431	0.095	120	66.2	1	0.33	763.8	22.6	27.9
14	BR10-03	s14	5.31	4.09	1.01	144	26	417	59	0.346	0.079	110	70.1	1	0.33	766.4	21.9	26.8
15	BR10-03	s15	4.14	3.19	0.86	91	106	291	306	0.311	0.091	127	117.8	1	0.33	742.6	22.8	28.6
16	BR10-03	s16	5.88	4.53	0.93	326	50	736	139	0.443	0.108	103	85.0	1	0.33	776.5	18.9	22.4
17	BR10-03	s17	6.69	5.16	0.88	138	18	441	98	0.313	0.080	114	140.0	1	0.33	789.5	16.3	18.7
18	BR10-03	s18	2.70	2.08	0.58	193	32	1028	294	0.188	0.062	107	110.9	1	0.33	704.2	21.8	27.6
19	BR10-03	s19	4.37	3.37	0.73	567	72	909	138	0.624	0.124	115	44.4	1	0.33	747.7	18.7	22.3
20	BR10-03	s20	7.42	5.72	0.98	158	41	414	54	0.382	0.111	114	14.6	1	0.33	800.2	16.7	19.1
21	BR10-03	s21	4.96	3.82	0.78	163	21	401	52	0.407	0.074	107	88.8	1	0.33	759.8	18.2	21.5
22	BR10-03	s22	7.85	6.06	3.78	328	105	565	121	0.580	0.223	127	8.9	1	0.33	806.2	53.7	94.2
23	BR10-03	s23	5.99	4.62	0.88	268	62	555	81	0.483	0.131	112	89.3	1	0.33	778.4	17.7	20.6
1	BR11-03	s1	3.79	2.92	0.65	697	117	2912	389	0.239	0.051	114	141.0	1	0.5	697.7	17.3	20.9
2	BR11-03	s2	12.73	9.82	1.29	533	73	1190	179	0.448	0.091	102	84.9	1	0.5	813.3	13.4	14.9
3	BR11-03	s3	11.97	9.23	1.25	144	18	411	53	0.351	0.064	101	52.8	1	0.5	806.8	13.5	15.1
4	BR11-03	s4	14.54	11.22	7.18	2032	324	4064	677	0.500	0.115	137	82.1	1	0.5	827.8	57.1	101.7
5	BR11-03	s5	2.69	2.08	0.55	570	83	3262	501	0.175	0.037	98	152.2	1	0.5	669.5	19.4	24.2
6	BR11-03	s6	2.47	1.90	0.54	884	133	4502	573	0.196	0.039	103	249.1	1	0.5	662.5	20.1	25.5
7	BR11-03	s7	2.14	1.65	0.50	535	73	1753	367	0.305	0.076	111	79.7	1	0.5	651.5	21.0	27.2
8	BR11-03	s8	3.76	2.90	0.69	742	95	2791	365	0.266	0.049	113	152.1	1	0.5	697.0	18.6	22.7
9	BR11-03	s9	2.19	1.69	0.51	655	183	1922	314	0.341	0.110	107	50.5	1	0.5	652.9	21.1	27.3
10	BR11-03	s10	5.56	4.29	0.81	692	90	4187	538	0.165	0.030	267	130.6	1	0.5	731.5	16.0	18.8
11	BR11-03	s11	1.90	1.46	0.50	616	106	2818	362	0.219	0.047	89	212.0	1	0.5	642.1	22.7	30.5
12	BR11-03	s12	4.58	3.53	0.73	1240	285	2620	511	0.473	0.143	104	117.6	1	0.5	714.1	16.8	20.0
13	BR11-03	s13	5.06	3.91	0.82	607	239	1600	530	0.379	0.195	86	102.6	1	0.5	723.1	17.4	20.7
14	BR11-03	s14	17.13	13.22	10.64	513	90	2143	365	0.239	0.058	122	161.2	1	0.5	846.0	71.2	159.0
15	BR11-03	s15	2.28	1.76	0.48	744	92	3084	411	0.241	0.044	96	130.0	1	0.5	656.1	19.4	24.5
16	BR11-03	s16	2.74	2.12	0.56	969	172	3504	445	0.277	0.060	111	126.6	1	0.5	670.9	19.2	24.0
17	BR11-03	s17	13.40	10.34	1.29	5392	694	5129</										

TABLE DR3. Primary magmatic CA-ID-TIMS U-Pb zircon geochronology of the Bergell Intrusion, Central Alps, adapted from Samperton *et al.* (2015), *Chemical Geology*.

Dates (Ma)												Composition					Isotopic Ratios										Analytical Notes and Crystal Details																
Analysis ID	206Pb/ 238U		206Pb/ ±2σ		207Pb/ 238U		207Pb/ ±2σ		206Pb/ 206Pb		Pb*	Pbc		Pb*/ Th/U		206Pb/ 204Pb		206Pb/ 208Pb		238U		238U		207Pb/ 235U		207Pb/ 206Pb		Corr.		Fragment			Grain										
	#	Fraction	<uncorr>	abs	<Th>	a	abs	%rel /	<Pa>	b	abs	<ThPa>	ab	abs	(pg)	c	(pg)	d	Pbc	e	(zircon)	f	204Pb	g	206Pb	h	<uncorr>	h	±2σ %	<Th>	ha	±2σ %	<Pa>	hb	±2σ %	<ThPa>	hab	±2σ %	coef.	Lab	Tracer	Geometry i	Texture j
BR10-04: tonalite from Preda Rosa (N 46.229929, E 9.698992)																																											
1	z1a	31.637	0.012	31.733	0.012	0.303	31.655	0.117	25.8	8.5	16.1	0.46	35.0	0.436	2154	0.1399	0.0049197	0.037	0.0049347	0.037	0.031667	0.37	0.04656	0.35	0.56	BSU	ET2535	M	H	13300													
2	z1b	31.707	0.013	31.803	0.013	0.303	31.722	0.163	25.6	12.1	13.3	0.53	25.1	0.576	1493	0.1849	0.0049306	0.042	0.0049456	0.042	0.031735	0.52	0.04656	0.50	0.50	BSU	ET2535	M	H	4500													
3	z2a	31.514	0.018	31.610	0.018	0.304	31.706	0.118	38.9	8.2	15.2	0.62	24.5	0.330	1560	0.1060	0.0049006	0.056	0.0049156	0.056	0.031718	0.38	0.04682	0.34	0.67	BSU	ET2535	T	H	20800													
4	z2b	31.612	0.023	31.708	0.023	0.303	31.893	0.135	45.8	9.7	11.5	0.49	23.3	0.376	1465	0.1207	0.0049159	0.073	0.0049309	0.073	0.031908	0.43	0.04695	0.41	0.39	BSU	ET2535	M	H	13875													
5	z3	31.534	0.012	31.630	0.012	0.304	31.645	0.057	32.8	3.9	58.5	0.54	109.2	0.368	6809	0.1180	0.0049037	0.037	0.0049186	0.037	0.031656	0.18	0.04670	0.16	0.60	BSU	ET2535	W	S	20400													
6	z4	31.751	0.012	31.847	0.012	0.302	31.834	0.086	30.8	6.3	46.4	0.85	54.5	0.528	3266	0.1692	0.0049376	0.038	0.0049525	0.038	0.031848	0.28	0.04666	0.26	0.38	BSU	ET2535	W	S	51104													
7	z5	31.321	0.011	31.417	0.011	0.306	31.440	0.096	33.2	7.2	22.8	0.45	50.3	0.200	3299	0.0643	0.0048705	0.034	0.0048854	0.036	0.031448	0.31	0.04671	0.30	0.37	BSU	ET2535	W	S,H	15700													
8	z6a	31.676	0.039	31.772	0.039	0.303	31.399	0.615	3.0	45.8	4.1	0.65	6.3	0.443	409	0.1420	0.0049258	0.124	0.0049407	0.123	0.031406	1.99	0.04612	1.90	0.73	Princeton	ET535	T	S	5000													
9	z6b	31.214	0.020	31.310	0.021	0.307	31.263	0.117	27.6	8.4	12.2	0.38	31.9	0.111	2173	0.0357	0.0048539	0.064	0.0048688	0.067	0.031268	0.38	0.04660	0.35	0.56	Princeton	ET535	T	S	9000													
10	z6c	31.507	0.020	31.603	0.020	0.304	31.448	0.194	19.6	14.4	6.8	0.34	19.8	0.356	1267	0.1141	0.0048994	0.063	0.0049144	0.063	0.031456	0.63	0.04644	0.60	0.49	Princeton	ET535	M	S	8700													
11	z6d	31.733	0.032	31.829	0.032	0.302	31.889	0.427	36.4	31.1	3.9	0.42	9.3	0.457	586	0.1466	0.0049347	0.100	0.0049497	0.100	0.031905	1.36	0.04677	1.30	0.63	Princeton	ET535	M	S	7150													
12	z7a	31.677	0.056	31.773	0.056	0.303	31.205	0.989	-12.1	74.7	1.7	0.43	4.0	0.443	265	0.1421	0.0049260	0.177	0.0049410	0.176	0.031213	3.22	0.04584	3.09	0.74	Princeton	ET535	T	H	2512													
13	z7b	31.824	0.088	31.920	0.088	0.301	31.343	1.595	-12.6	119.4	1.7	0.70	2.4	0.559	163	0.1794	0.0049489	0.278	0.0049638	0.276	0.031350	5.17	0.04583	4.94	0.83	Princeton	ET535	M	H	4050													
14	z7c	31.693	0.040	31.789	0.040	0.303	31.442	0.651	5.0	48.4	1.9	0.32	5.9	0.497	374	0.1594	0.0049285	0.128	0.0049453	0.127	0.031450	2.10	0.04616	2.01	0.76	Princeton	ET535	M	H	3850													
15	z7d	31.788	0.029	31.884	0.029	0.302	31.962	0.394	37.8	28.7	4.6	0.45	10.1	0.528	628	0.1694	0.0049434	0.091	0.0049583	0.090	0.031979	1.25	0.04680	1.20	0.61	Princeton	ET535	M	H	11000													
16	z8a	31.464	0.033	31.560	0.033	0.305	31.721	0.370	43.9	27.0	7.9	0.81	9.8	0.308	645	0.0987	0.0048928	0.104	0.0049077	0.104	0.031734	1.19	0.04692	1.13	0.60	Princeton	ET535	M	H	18225													
17	z8b	31.368	0.021	31.464	0.021	0.306	31.591	0.221	41.3	16.2	6.0	0.37	16.1	0.170	1084	0.0544	0.0048779	0.068	0.0048928	0.068	0.031602	0.71	0.04686	0.68	0.54	Princeton	ET535	T	H	1375													
18	z8c	31.403	0.018	31.499	0.018	0.305	31.529	0.069	33.8	4.7	28.9	0.48	60.0	0.239	3922	0.0766	0.0048833	0.057	0.0048983	0.058	0.031539	0.22	0.04672	0.19	0.57	Princeton	ET535	M	H	19575													
BR10-03: tonalite from Lago di Mezzola (N 46.177708, E 9.440609)																																											
19	z1a	31.346	0.077	31.442	0.076	0.306	32.587	1.263	117.8	88.5	2.5	1.25	2.0	0.427	142	0.1370	0.0048744	0.245	0.0048893	0.243	0.032614	3.94	0.04840	3.75	0.77	BSU	ET2535	M	O	10800													
20	z1b	31.192	0.056	31.288	0.055	0.308	31.114	1.181	17.7	89.7	1.6	0.69	2.3	0.326	164	0.1045	0.0048504	0.179	0.0048653	0.177	0.031177	3.85	0.04641	3.73	0.70	BSU	ET2535	M	O	10800													
21	z2a	31.141	0.015	31.237	0.015	0.308	31.192	0.256	27.8	19.3	7.5	0.62	12.1	0.372	767	0.1193	0.0048424	0.047	0.0048574	0.047	0.031197	0.83	0.04660	0.80	0.65	BSU	ET2535	M	O	16250													
22	z2b	31.121	0.023	31.217	0.023	0.308	32.620	0.340	137.2	23.9	3.5	0.44	8.0	0.293	522	0.0940	0.0048393	0.073	0.0048543	0.073	0.032647	1.06	0.04880	1.02	0.57	BSU	ET2535	T	O	10625													
23	z4a	31.179	0.017	31.275	0.017	0.308	31.616	0.339	57.6	25.1	4.1	0.46	8.9	0.366	573	0.1173	0.0048484	0.056	0.0048633	0.056	0.031626	1.09	0.04719	1.05	0.67	BSU	ET2535	M	O	15600													
24	z4b	30.770	0.016	30.866	0.017	0.312	31.128	0.322	51.4	24.2	5.0	0.49	10.2	0.123	696	0.0395	0.0047846	0.051	0.0047995	0.054	0.031311	1.05	0.04706	1.01	0.72	BSU	ET2535	T	O	3600													
25	z5a	31.476	0.055	31.571	0.055	0.305	30.971	1.167	-15.3	89.0	2.4	0.75	3.2	0.436	213	0.1400	0.0048946	0.176	0.0049095	0.174	0.030972	3.83	0.04577	3.68	0.83	Princeton	ET535	M	O,S	9200													
26	z5b	31.469	0.067	31.565	0.067	0.305	31.752	1.229	45.9	89.8	2.8	0.95	2.9	0.397	200	0.1274	0.0048935	0.214	0.0049085	0.212	0.031765	3.93	0.04696	3.76	0.83	Princeton	ET535	M	O,S	9200													
27	z6a	31.203	0.047	31.299	0.046	0.307	30.907	0.772	0.5	58.5	3.1	0.65	4.7	0.376	314	0.1205	0.0048521	0.149	0.0048671	0.148	0.030907	2.54	0.04608	2.42	0.78	Princeton	ET535	T	S	6500													
28	z6b	31.389	0.025	31.485	0.025	0.306	31.594	0.385	39.9	28.3	7.0	0.71	9.9	0.562	605	0.1801	0.0048811	0.079	0.0048960	0.078	0.031605	1.24	0.04684	1.18	0.72	Princeton	ET535	M	S	8000													
29	z6c	31.307	0.028	31.403	0.028	0.306	31.593	0.393	46.0	28.8	8.2	0.87	9.4	0.385	608	0.1235	0.0048684	0.089	0.0048833	0.088</td																							

47	z13a	30.669	0.020	30.765	0.020	0.313	30.837	0.067	36.4	4.6	44.6	0.74	60.3	0.194	3989	0.0623	0.0047689	0.065	0.0047838	0.066	0.030836	0.22	0.04677	0.19	0.55	Princeton	ET535	T	M	35000
48	z13b	30.715	0.017	30.811	0.017	0.312	30.973	0.115	43.6	8.5	20.2	0.66	30.6	0.213	2022	0.0684	0.0047760	0.054	0.0047909	0.055	0.030974	0.38	0.04691	0.35	0.50	Princeton	ET535	T	O	10500
49	z14	30.864	0.021	30.960	0.021	0.311	31.160	0.253	46.6	18.8	28.6	2.15	13.3	0.213	887	0.0683	0.0047992	0.067	0.0048142	0.067	0.031164	0.83	0.04697	0.78	0.64	Princeton	ET535	W	O	45000
50	z5	30.850	0.019	30.946	0.019	0.311	31.049	0.147	39.0	10.9	22.5	0.94	23.8	0.251	1563	0.0804	0.0047971	0.061	0.0048120	0.062	0.031051	0.48	0.04682	0.45	0.51	Princeton	ET535	W	O	24150
51	z6	30.683	0.026	30.779	0.026	0.313	30.944	0.322	43.8	24.1	45.1	4.29	10.5	0.248	701	0.0794	0.0047710	0.084	0.0047860	0.084	0.030944	1.06	0.04691	1.01	0.62	Princeton	ET535	W	M	30550
52	z7	30.795	0.019	30.891	0.019	0.312	30.959	0.080	36.2	5.7	27.7	0.56	49.6	0.293	3192	0.0940	0.0047886	0.061	0.0048035	0.061	0.030959	0.26	0.04677	0.24	0.50	Princeton	ET535	M	M	14400
53	z8a	30.850	0.016	30.946	0.016	0.311	31.043	0.060	38.6	4.1	67.0	0.99	67.9	0.252	4421	0.0809	0.0047971	0.052	0.0048120	0.053	0.031045	0.20	0.04681	0.17	0.60	Princeton	ET535	T	O	23100
BR10-05: hybridized granitoid from Bagni di Masino (N 46.236622, E 9.604717)																														
54	z1	30.842	0.009	30.938	0.010	0.311	31.154	0.066	47.8	4.9	44.0	0.51	86.4	0.226	5608	0.0726	0.0047959	0.030	0.0048108	0.031	0.031158	0.21	0.04699	0.20	0.34	BSU	ET2535	T	O	14400
55	z10a	30.791	0.029	30.887	0.029	0.311	30.913	0.230	32.9	17.0	7.2	0.46	15.6	0.247	1029	0.0794	0.0047879	0.095	0.0048028	0.095	0.030913	0.75	0.04670	0.71	0.54	Princeton	ET535	T	O	1625
56	z10b	30.929	0.024	31.025	0.024	0.310	31.248	0.154	48.4	10.5	8.3	0.32	26.2	0.316	1683	0.1014	0.0048094	0.079	0.0048243	0.078	0.031253	0.50	0.04701	0.44	0.80	Princeton	ET535	C	M	5250
57	z10c	30.751	0.024	30.847	0.024	0.312	30.987	0.266	41.9	19.8	21.1	1.65	12.8	0.241	850	0.0772	0.0047816	0.079	0.0047966	0.079	0.030988	0.87	0.04688	0.83	0.56	Princeton	ET535	T	O	4500
58	z4	30.755	0.023	30.851	0.023	0.312	30.895	0.255	34.4	18.4	18.8	1.80	10.4	0.228	693	0.0731	0.0047822	0.076	0.0047972	0.076	0.030895	0.84	0.04673	0.77	0.94	BSU	ET2535	T	O	10000
59	z6	30.760	0.009	30.856	0.009	0.312	30.964	0.116	39.3	8.8	68.1	2.19	31.2	0.303	1991	0.0972	0.0047831	0.029	0.0047981	0.030	0.030964	0.38	0.04683	0.37	0.47	BSU	ET2535	W	O	22500
60	z7	30.829	0.008	30.924	0.008	0.311	30.987	0.078	35.9	5.9	40.9	0.59	69.4	0.292	4430	0.0936	0.0047937	0.026	0.0048087	0.027	0.030988	0.26	0.04676	0.24	0.50	BSU	ET2535	W	O	20000
61	z8b	30.881	0.035	30.976	0.035	0.311	30.401	0.562	-14.9	43.3	4.8	0.78	6.2	0.277	415	0.0889	0.0048018	0.113	0.0048168	0.112	0.030393	1.88	0.04578	1.79	0.77	Princeton	ET535	M	M	2200
62	z8c	30.829	0.021	30.924	0.021	0.311	30.786	0.210	20.0	15.9	4.9	0.26	19.0	0.260	1246	0.0835	0.0047937	0.067	0.0048087	0.067	0.030784	0.69	0.04645	0.66	0.51	Princeton	ET535	T	O	2600
63	z8d	30.890	0.046	30.986	0.046	0.311	31.026	0.743	34.1	55.6	2.6	0.54	4.8	0.296	328	0.0948	0.0048033	0.150	0.0048182	0.148	0.031027	2.43	0.04673	2.32	0.75	Princeton	ET535	M	M	1600
64	z9a	30.671	0.022	30.767	0.022	0.313	30.763	0.250	30.4	18.7	6.2	0.43	14.4	0.223	962	0.0715	0.0047692	0.073	0.0047841	0.074	0.030760	0.82	0.04665	0.78	0.64	Princeton	ET535	T	O	3900
65	z9c	30.924	0.017	31.020	0.017	0.310	30.589	0.282	-3.1	22.5	15.1	1.12	13.5	0.355	866	0.1140	0.0048086	0.055	0.0048236	0.055	0.030584	0.94	0.04601	0.93	0.13	Princeton	ET535	C	M	4125
BR11-03: granodiorite from Forno (N 46.335150, E 9.717360)																														
66	z1	30.744	0.021	30.840	0.021	0.312	31.064	0.235	48.4	17.5	49.3	3.50	14.1	0.178	951	0.0570	0.0047806	0.069	0.0047956	0.069	0.031066	0.77	0.04700	0.73	0.60	Princeton	ET535	W	O	40250
67	z5	30.864	0.017	30.960	0.017	0.311	31.037	0.066	37.0	4.6	50.1	0.83	60.5	0.217	3977	0.0696	0.0047993	0.054	0.0048142	0.055	0.031039	0.22	0.04678	0.19	0.55	Princeton	ET535	W	M	31086
68	z6a	30.675	0.022	30.771	0.023	0.313	30.754	0.265	29.4	20.2	6.1	0.48	12.8	0.126	879	0.0403	0.0047699	0.072	0.0047848	0.074	0.030751	0.87	0.04663	0.84	0.52	Princeton	ET2535	T	O	4000
69	z6b	30.684	0.057	30.780	0.056	0.313	31.055	0.956	52.4	71.4	12.3	3.63	3.4	0.134	245	0.0430	0.0047712	0.187	0.0047861	0.184	0.031057	3.13	0.04708	2.99	0.77	Princeton	ET2535	M	M	9600
70	z6c	30.756	0.076	30.852	0.075	0.312	30.969	1.085	40.1	80.7	3.2	0.94	3.4	0.192	241	0.0616	0.0047824	0.247	0.0047973	0.244	0.030970	3.56	0.04684	3.37	0.77	Princeton	ET2535	T	O	5400
71	z6d	30.593	0.036	30.689	0.036	0.314	30.686	0.558	30.5	42.5	3.7	0.58	6.4	0.126	446	0.0403	0.0047570	0.119	0.0047719	0.118	0.030682	1.84	0.04665	1.77	0.65	Princeton	ET2535	M	O	6000
72	z7a	30.912	0.030	31.008	0.031	0.310	31.102	0.049	38.3	2.3	95.8	0.51	186.9	0.263	12091	0.0844	0.0048068	0.099	0.0048218	0.099	0.031104	0.16	0.04681	0.09	0.84	Princeton	ET2535	M	M	28500
73	z7b	30.809	0.022	30.905	0.023	0.311	31.014	0.037	39.4	2.0	95.5	0.40	237.9	0.189	15714	0.0608	0.0047908	0.073	0.0048057	0.073	0.031015	0.12	0.04683	0.08	0.78	Princeton	ET2535	T	O	16900
74	z8a	30.822	0.035	30.917	0.035	0.311	30.681	0.401	12.2	30.4	12.0	1.41	8.5	0.201	580	0.0646	0.0047926	0.114	0.0048076	0.113	0.030677	1.33	0.04630	1.26	0.60	Princeton	ET2535	T	O	4592
75	z8b	30.923	0.028	31.019	0.028	0.310	30.995	0.111	29.1	7.7	20.4	0.51	40.2	0.314	2581	0.1006	0.0048085	0.090	0.0048235	0.090	0.030996	0.36	0.04663	0.32	0.58	Princeton	ET2535	C	M	16200
76	z8c	30.860	0.013	30.956	0.013	0.311	31.041	0.080	37.6	5.7	28.4	0.60	47.5	0.300	3052	0.0961	0.0047986	0.043	0.0048136	0.043	0.031042	0.26	0.04679	0.24	0.60	Princeton	ET2535	C	M	13950
77	z9a	30.848	0.012	30.944	0.012	0.311	30.904	0.093	27.8	6.9	11.2	0.27	41.3	0.211	2730	0.0677	0.0047967	0.038	0.0048117	0.040	0.030903	0.31	0.04660	0.29	0.53	Princeton	ET2535	T	O	3000
78	z9b	30.888	0.021	30.984	0.021	0.311	31.089	0.169	39.3	12.5	6.0	0.28	21.6	0.218	1434	0.0701	0.0048030	0.067	0.0048179	0.068	0.031092	0.55	0.04683	0.52	0.49	Princeton	ET2535	T	O	2438
79	z9c	30.901	0.068	30.997	0.067	0.310	31.200	1.234	46.9	91.8	2.7	0.97	2.8	0.232	199	0.0745	0.0048050	0.220	0.0048199	0.217	0.031204	4.02	0.04698	3.84	0.81	Princeton	ET2535	T	O	3450
80	z9d	30.918	0.021	31.014	0.021	0.310	31.053	0.152	34.1	11.4	11.2	0.46	24.3	0.210	1610	0.0674	0.0048077	0.067	0.0048226	0.067	0.031055	0.50	0.04672	0.48	0.37	Princeton	ET2535	M	M	6250
BR10-08: granodiorite from																														

a Corrected for initial Th/U disequilibrium using radiogenic ^{208}Pb , $(\text{Th}/\text{U})_{\text{zircon}}$ and a mean $(\text{Th}/\text{U})_{\text{zircon-melt}}$ partition coefficient ratio of 0.117 (from Nardi et al., 2013, Group 2+3 granitoids).

b Corrected for initial Pa/U disequilibrium using initial fraction activity ratio $[231\text{Pa}]/[235\text{U}] = 1.1$.

c Total mass of radiogenic Pb.

d Total mass of common Pb. Princeton Pbc IC: $^{206}\text{Pb}/^{204}\text{Pb} = 18.417 \pm 0.180$, $^{207}\text{Pb}/^{204}\text{Pb} = 15.478 \pm 0.166$; $^{208}\text{Pb}/^{204}\text{Pb} = 37.809 \pm 0.600$ (1σ).

BSU Pbc IC: $^{206}\text{Pb}/^{204}\text{Pb} = 18.030 \pm 0.127$, $^{207}\text{Pb}/^{204}\text{Pb} = 15.511 \pm 0.094$, $^{208}\text{Pb}/^{204}\text{Pb} = 37.564 \pm 0.270$ (1σ).

e Ratio of radiogenic Pb (including ^{208}Pb) to common Pb.

f Th contents calculated from radiogenic ^{208}Pb and the $^{207}\text{Pb}/^{206}\text{Pb}$ date of the sample, assuming concordance between U-Th and Pb systems.

g Measured ratio corrected for fractionation and spike contribution only.

h Measured ratios corrected for fractionation, tracer and blank.

i Geometry of microsample fragment: T=tip, M=mixed tip+core, C=core, W=whole grain.

j Primary CL texture/crystal zoning: O=oscillatory, H=homogenous, S=sector, C=core, M=mixed O+C.

k Zircon fragment size (μm^2) calculated from CL image dimensions.

l % relative difference between Th-corr and Th-uncorr $^{206}\text{Pb}/^{238}\text{U}$ date ($\Delta t = 100 \times (\text{Thcorr} - \text{Thuncorr}) / (\text{Thuncorr})$)

TABLE DR4. Bergell whole-rock geochemistry

Analyte (wt.%) BR10-04 BR10-03 BR11-03

SiO ₂	60.75	57.13	64.91
Al ₂ O ₃	16.75	17.13	16.1
Fe ₂ O ₃ (T)	6.37	7.06	3.73
MnO	0.122	0.125	0.074
MgO	3.13	3.39	1.73
CaO	6.85	7.09	3.62
Na ₂ O	3.04	3.05	3.71
K ₂ O	2.05	2.19	3.81
TiO ₂	0.634	0.732	0.413
P ₂ O ₅	0.16	0.23	0.25
LOI	1.07	0.97	0.56
Zr (ppm)	141	154	174